



Original Paper

Chemometric Differentiation of Oil Families and Their Potential Source Rocks in the Gulf of Suez

W. Sh. El Diasty^{1,5}, S. Y. El Beialy,¹ A. R. Mostafa,² A. A. Abo Ghonaim,¹
and K. E. Peters^{3,4}

Received 18 May 2019; accepted 9 October 2019
Published online: 18 October 2019

An oil–oil and oil–source rock correlation study was carried out using chemometric methods applied to geochemical data for 123 Upper Cretaceous–Lower Miocene putative source rock and 46 crude oil samples from the Gulf of Suez Rift basin. The Gulf of Suez has many organic-rich intervals. The pre-rift source units, such as the Brown Limestone and Thebes formations, contain very good-to-excellent organic content, whereas the Miocene rocks are rated fair to good. HI and T_{\max} pyrolysis data indicate variable kerogen type and maturation histories where most of the analyzed samples occur along the Type II and Type II/III kerogen pathways from immature to the main stage of oil window with %R_o < 0.9. Carbon isotope ratios' biomarker data for the bitumen samples indicate predominantly anoxic source rock depositional conditions with substantial algal/bacterial marine and a minor terrigenous organic matter. The Gulf of Suez oils exhibit a wide range of chemical composition from heavy-to-medium gravity and moderate-to-high sulfur content. These oils originated from carbonate/marl source rocks rich in lipids from phytoplankton/benthic algae and bacteria with less contribution of terrigenous organic debris, deposited under anoxic conditions with different thermal maturity histories equivalent to at least the early oil window. Chemometrics using 16 source-related biomarker and isotope ratios identifies six genetic families in the Gulf of Suez. The oil families share common characteristics where the precursor organic matter was deposited in a restricted marine environment with limited land-derived organic matter. The major factor that greatly modifies oil composition in the Gulf of Suez is thermal maturation. However, migration history and spatial and temporal organofacies' variations of the presumed source rocks are also important. The overall geochemical similarity of the Gulf of Suez oils confirms the mixed nature of these fluids and suggests that no single source rock horizon is likely to have sourced the oil in this promising province. Based on oil–source correlation data and a decision tree chemometric model, the Brown Limestone, Esna, Thebes, and Nukhul formations are the effective source rocks for oil families III, IV, and V, whereas none of the source rock extracts has been assigned for Family I or VI oils.

KEY WORDS: Oil–source correlation, Chemometrics, Oil families, Gulf of Suez Rift.

¹Geology Department, Faculty of Science, Mansoura University, Mansoura 35516, Egypt.

²Department of Environmental Sciences, Faculty of Science, Alexandria University, Alexandria 21568, Egypt.

³Schlumberger, Mill Valley, CA 94941, USA.

⁴School of Earth Sciences, Stanford University, Stanford, CA 94305, USA.

⁵To whom correspondence should be addressed; e-mail: awaleed@mans.edu.eg

INTRODUCTION

The Gulf of Suez (also known as Clysmic after Clysmia, the old Roman name of the Suez city) is one of the most prolific sedimentary basins for oil production in Egypt and the best studied continental rift in the world. It is the subject of many excellent re-

views of rift basins (e.g., Bosworth 1985; Steckler 1985; Moretti and Chénet 1987; Patton et al. 1994; Schütz 1994; Bosworth and McClay 2001; Moustafa 2002; Alsharhan 2003; Khalil and McClay 2016). Recent hydrocarbon exploration and superb rift margin exposures in the Eastern Desert and Sinai and on both sides of the modern Gulf of Suez have enabled comprehensive reviews, synthesis and original data on rift tectonostratigraphy (Schütz 1994; Lambaise and Bosworth 1995; Bosworth and McClay 2001), the dynamic tectonic evolution and rift geometry (Moustafa 1976; Angelier 1985; Moretti and Colletta 1987; Colletta et al. 1988; Bosworth 1995; Bosworth and Durocher 2017), pre-rift control on fault linkage (McClay et al. 1998; Younes and McClay 2002), carbonate platform development (Bosence 2012), and sedimentation in the rift system (Richardson and Arthur 1988; Darwish and El-Araby 1993; Patton et al. 1994; Alsharhan and Salah 1995; Moustafa and Khalil 1995; Purser and Bosence 1998; Peijs et al. 2012).

Many, but not all, rift basins contain excellent petroleum source rocks in addition to an unpredictable amount of hydrocarbons based on their area and sediment volume (Katz, 1995). The geochemical characteristics of oils and source rocks from the Gulf of Suez Province have been studied by many workers, including Rohrback (1983), Elzarka and Mostafa (1988), Mostafa (1993), Alsharhan and Salah (1995, 1997), Robison (1995), Barakat et al. (1997), Khavari-Khorasani et al. (1998), Mostafa (1999), Wever (2000), Bakr and Wilkes (2002), Alsharhan (2003), Younes (2003), Barakat et al. (2005), Younes and Philp (2005), Sharaf et al. (2007), El Atfy et al. (2014), El Diasty and Peters (2014), and El Diasty et al. (2014, 2015a, b). Most of these syntheses are case studies, and their findings focused on geochemical character and the origin of reservoir hydrocarbons without definitive oil–source correlations. This is may be a consequence of the lack of the proper source rock sampling or inappropriate geochemical data.

Chemometric methods, such as principal component analysis (PCA), hierarchical cluster analysis (HCA), and soft independent modeling of class analogy (SIMCA), can be used to determine reliable oil–source and oil–oil relationships (Zumberge et al. 2005; Peters et al. 2005, 2007, 2013, 2016; El Diasty et al. 2016, 2017a, 2018, 2019a; Wang et al. 2016, 2018; Alizadeh et al. 2017). The efficiency of chemometrics over most conventional diagrams, such as bivariate plots, results from the capacity to

reduce the dimensionality of multivariate data to into few key parameters or principal components (Peters et al. 2016; Wang et al. 2018).

This study aims to improve understanding of the genetic relationships among crude oils and source rocks in the Gulf of Suez Basin using multiple approaches, e.g., stable carbon isotope compositions, and saturated and aromatic biomarker signatures. In addition, we differentiate genetic oil families using a chemometric decision tree and principal component analysis (Pirouette[®]) and InStep[™] software (Infometrix[®]) to infer the source rocks for the families.

GEOLOGIC SETTING

The Gulf of Suez basin is about 19–32 km (12–20 miles) wide and 314 km (195 miles) long from its head at the city of Suez to the south at Ras Mohammed near the junction with the northern Red Sea (Fig. 1). The basin is an aborted continental rift that originated from Afar (Afro-Arabian Rift System) plume-related events. The NW–SE Clysmic rift trend, the northwestern extension of the Red Sea, generally formed as a result of rupturing of the continental lithosphere associated with upwelling from asthenosphere, which resulted in geological conditions favorable for hydrocarbon generation and accumulation. The Suez Rift, in addition to the left lateral Aqaba transform, is classified with those where no oceanic crust formed (Sellwood and Netherwood 1984; Bosworth 1985; Steckler 1985; Colletta et al. 1988). The dying out of the Suez Rift and activation of the Aqaba transform can be explained by the presence of stronger Mediterranean oceanic lithosphere to the north of the Gulf of Suez, which precludes northward propagation and leads to the transfer of motion along the Aqaba rift belt (Colletta et al. 1988). These two rift systems seem to be contemporaneous and initiated during Late Oligocene–Early Miocene time ($^{40}\text{Ar}/^{39}\text{Ar} \sim 24\text{--}22$ Ma; Garfunkel and Bartov 1977; Bosworth and Stockli 2016). As in many intra-cratonic rifts, extension within the Suez Rift was accommodated through displacement on low-angle normal faults that define a series of horsts and large-scale half-grabens (tilted blocks) that run subparallel to the border faults and were buried by Upper Miocene and Pliocene sediments (Moustafa 1976, 2002; Bosworth 1995, 2015; Bosworth and Durocher 2017).

The dip direction changes twice from north to south along the Suez Rift based on changes in half-



Fig. 1. Location map of the Gulf of Suez shows locations of the studied oilfields.

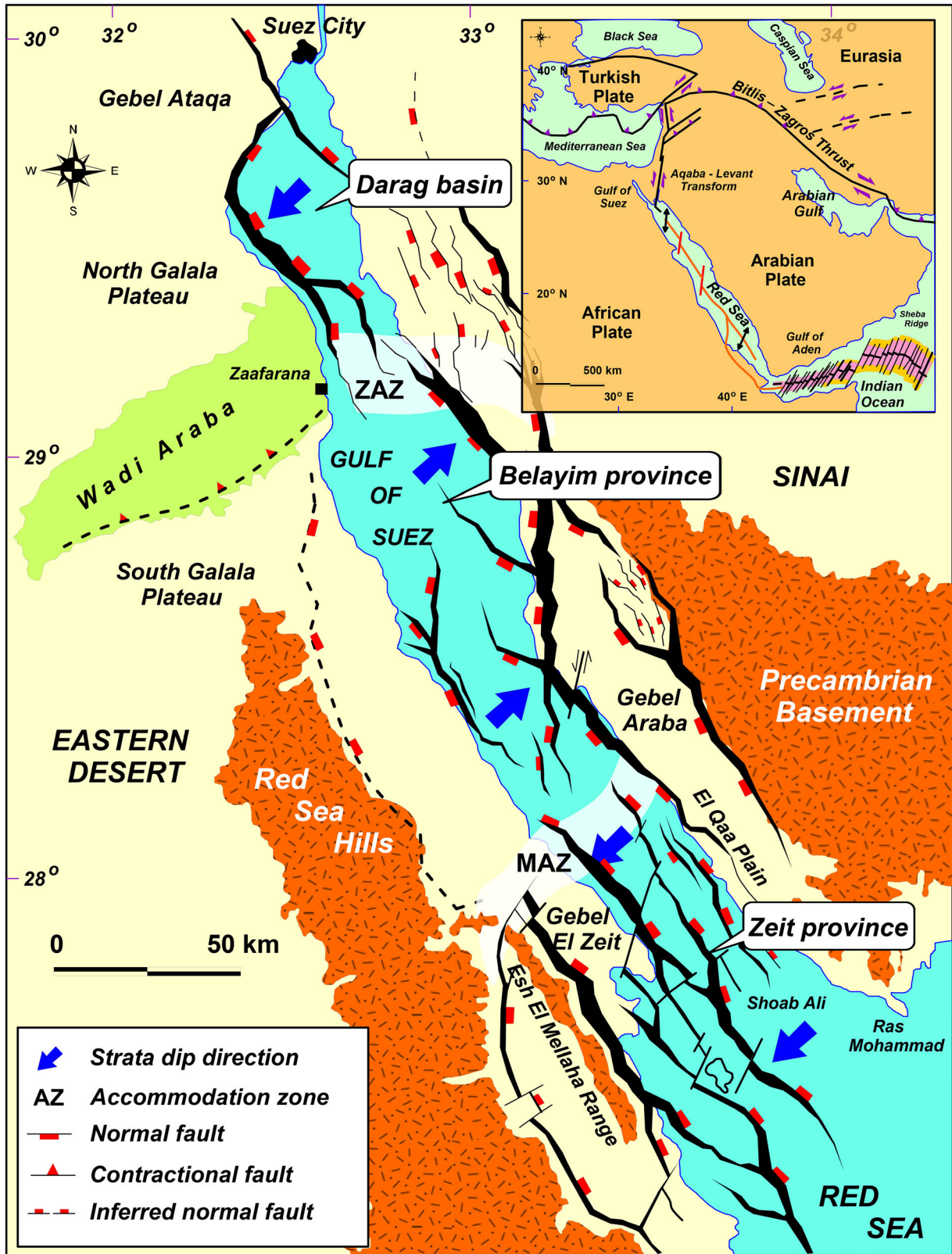
grabens and fault location or polarity. It is believed that these changes in dip polarity along strike are related to initial reactivation of preexisting regional Precambrian shear zones by Late Oligocene–Early Miocene extension. The region separating opposing-dip domains is called an accommodation zone, or twist zone without any transverse faults, or hinge zone (Moustafa 1976; Bosworth 1985; Morley et al. 1990; Patton et al. 1994; Younes and McClay 2002). Consequently, three major tectonic domains are evident in the Gulf of Suez, including the northern Darag basin, the central Belayim Province, and the southern Zeit Province (Fig. 2). The northern Darag basin looks like the southern basin, although it is much narrower. The southern Zeit Province, with its main NE-dipping basin-bounding fault, thickens toward the SW in each rotated fault block (Bosworth and Durocher 2017). Alternatively, in the central Belayim Province the geometry is reversed, with strata dipping to the NE and the bounding fault dipping to the SW (Fig. 2).

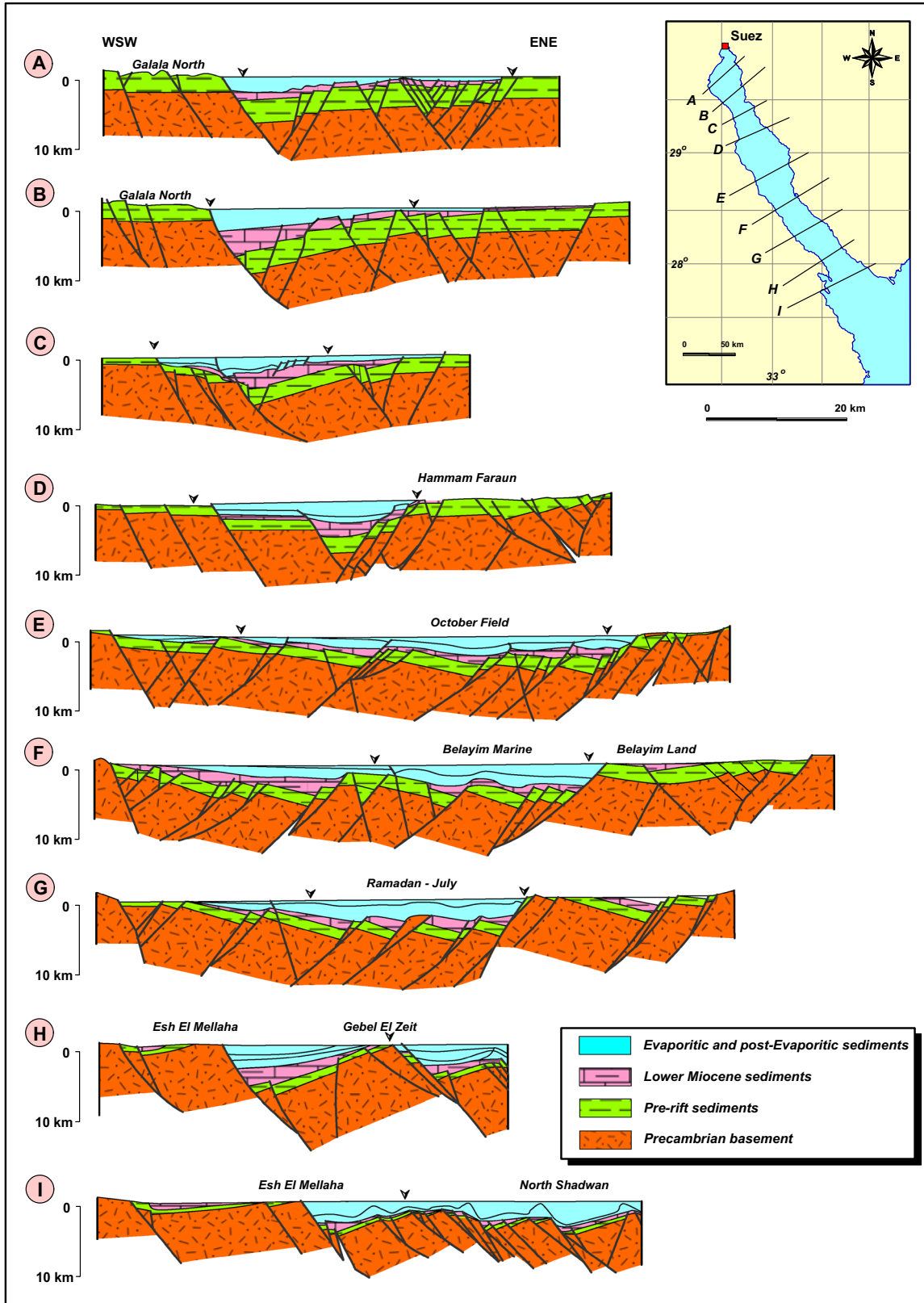
Although it appears simple with closely symmetrical shoulders, the inner structure of the Suez Rift has asymmetrical fault blocks (Fig. 3). When two opposite-dipping bounding faults merge and cross at depth, one of them becomes locked. Such locking prevents the simultaneous propagation of opposite-dipping faults and the formation of symmetrical grabens (Moretti and Colletta 1987; Colletta et al. 1988; Khalil and McClay 2001). However, the overall variation in extension along the Suez Rift is variable; for instance, the higher the extension, the smaller the block size, and the greater the tilt angle. The fault block size is 50 km wide in the Darag Basin, 20 km in the central Belayim Province, and only 15 km in the southern Zeit Province (Colletta et al. 1988). The Gulf of Suez opened in a scissor-like movement (differential extension), and the structure of the Suez Rift varies from south to north (Fig. 3). The differential extension of the rift varies from about 20 km in the southern basin (Gebel El Zeit area) to 4–5 km in the north (Darag Basin). The southward widening of the rift mainly results from the counterclockwise rotation of the Sinai plate in relation to the African plate (Angelier 1985).

The complete stratigraphic section of the Gulf of Suez can be divided into three mega-sequences: pre-rift, syn-rift and post-rift (Fig. 4; Garfunkel and Bartov 1977; Darwish and El-Araby 1993; Patton et al. 1994; Bosworth et al. 1998; Khalil and McClay 2001).

Fig. 2. Interpretation of major faults and shear zones in the Gulf of Suez area. ZAZ, Zaafarana accommodation zone; MAZ, Morgan accommodation zone (modified after Bosworth and McClay 2001). ▶

The pre-rift mega-sequence sedimentary record above the Precambrian crystalline basement ranges in age from Cambrian to Oligocene (Fig. 4). The Neoproterozoic crystalline basement is unconformably overlain by a thick series of Paleozoic to Lower Cretaceous shallow marine to continental non-fossiliferous sandstones (informally known as the “Nubian Sandstones”). These sandstones consist of four units arranged in ascending order: Nubia-D and Nubia-C, Araba and Naqus (Early Paleozoic Cambrian–Ordovician), Nubia-B Um Bogma, Abu Durba and Rod El Hamal (Carboniferous–Permian), and Nubia-A Qiseib and Malha formations (Triassic–Lower Cretaceous). In addition, these units are medium- to coarse-grained siliciclastic-dominated succession (Nubia-A, Nubia-C, and Nubia-D units are predominantly cross-bedded sandstone with thin interbeds of shale, while Nubia-B is a dark shale) several hundred meters thick (Sellwood and Netherwood 1984; Evans 1988; Darwish and El-Araby 1993; Patton et al. 1994; Schütz 1994; Khalil and McClay 2001). Unconformably above the Nubian sandstones lies a series of mixed marine siliciclastic and carbonate rocks of Cenomanian to Santonian age known as Nazzazat Group. This Cretaceous sequence consists of four formations: Raha (Cenomanian), Abu Qada (Cenomanian), Wata (Turonian), and Matulla (Coniacian–Santonian). From the Cenomanian through the Turonian, deposition took place in a restricted, shallow marine setting with more marginal marine and littoral environments increasing to the south (Schütz 1994). During the early Campanian, a major sea transgression inundated much of the northern Arabian–Nubian platform. The youngest Upper Cretaceous deposits are subdivided into the Brown Limestone or Duwi Formation (lower Campanian) and the Sudr Formation (Maastrichtian–Upper Campanian). The Campanian–Maastrichtian environment of deposition varies from marine to inner sublittoral, giving rise to various lithotypes of predominantly limestone with interbeds of highly calcareous shale. The Brown Limestone lithological characters represent a special marine condition, but the conformably overlying snow-white chalks of the Sudr Formation confirm open-marine deposition (Schütz 1994). These are in turn overlain by soft fossiliferous





◀ **Fig. 3.** Serial balanced cross sections across the Gulf of Suez Rift illustrate two changes of regional dip along the Gulf from north to south (modified after Colletta et al. 1988). The coastline is indicated by arrows. For locations, see inset.

shale of the Paleocene Esna Formation and the Eocene carbonate succession of the Thebes Formation (Patton et al. 1994; McClay et al. 1998). The uppermost pre-rift strata consist of sporadically developed continental reddish limestones, sandstones, and shales of the Tayiba (or Abu Zenima) Formation. After Oligocene exposure, graben subsidence commenced, accompanied by intrusion and eruption of basaltic rocks (Sellwood and Netherwood 1984). Basalt flows are abundant in the northern part of the Suez graben, and their position between the underlying Paleogene and overlying Neogene likely indicates the beginning of renewed foundering of the Suez Rift.

The syn-rift Miocene mega-sequence of the Gulf of Suez is commonly subdivided into two groups: (1) the basal Lower Miocene Gharandal Group (Fig. 4) and (2) the overlying Middle–Upper Miocene Ras Malaab Group. Both groups are important, the lower containing organic-rich source rocks and well-defined reservoirs deposited under favorable structural settings, and the upper one providing excellent seal for pre-rift and Miocene targets (Alsharhan 2003). The cumulative thickness of these two groups is almost twice that of the pre-Miocene rock units, which indicates a predominantly restricted depositional environment in a rapidly subsiding graben (Steckler 1985). Sediments of the Gharandal Group are widespread and rather uniform characteristics in surface outcrops and subsurface throughout the rift and can be differentiated into three stratigraphic units: the lower Nukhul Formation, the middle Rudeis Formation, and the upper Kareem Formation (Fig. 4). This group consists of open-marine *Globigerina*-bearing marls and shales and heterogeneous and laterally discontinuous beds of conglomeratic and brecciated sandstones at base of the syn-rift section (Sellwood and Netherwood 1984; Bosworth 2015). The overlying evaporitic Ras Malaab Group (Belayim, South Gharib, and Zeit formations) consists of anhydrite, gypsum, and salt alternating with marl, shale, fossiliferous limestone, and coarse clastics. The presence of thick evaporites in this group is likely a response to the developing uplifts of the rift should-

ers, which restricted access to the Mediterranean Sea (Steckler 1985) together with a falling sea level (Steckler et al. 1988).

MATERIALS AND METHODS

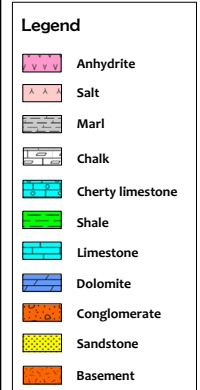
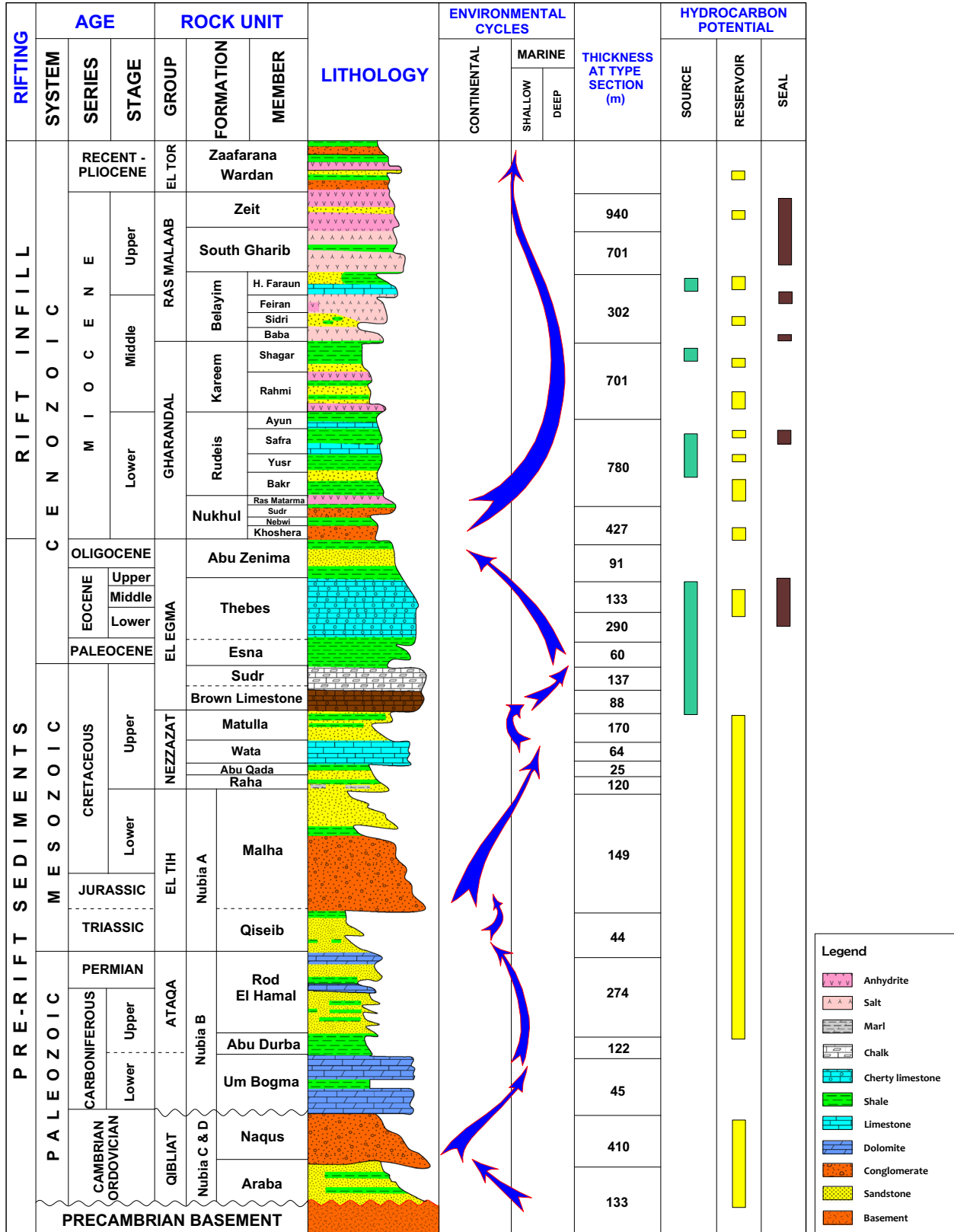
This regional study consists of 46 crude oil samples and 123 rock samples based on data from 19 representative on- and offshore oilfields in the Gulf of Suez graben. The crude oil samples were collected from reservoirs ranging in age from Early Cretaceous (Nubia) to the Middle Miocene (Kareem). Cuttings samples from 22 exploration wells were selected from the most likely source rocks for crude oils reservoired in the Gulf of Suez Province. Locations of the studied oilfields are shown in Fig. 1.

The organic richness, kerogen type, and the thermal maturity of the disseminated organic matter (Espitalié et al. 1977; Peters 1986; Peters and Cassa 1994) for the studied rock samples were determined using a Rock-Eval 6 analyzer (Vinci Technologies) according to the standard technique outlined by Béhar et al. (2001). The total organic carbon (TOC) content was measured by combustion in an induction furnace in a flow of oxygen through a LECO C230 carbon analyzer.

Thirty-nine organic-rich rock samples from different intervals characterized by various lithologies were selected for extraction and biomarker analyses. Pulverized (passed through a 40-mesh sieve) rock samples were extracted using a mixture of CH_2Cl_2 and CH_3OH (9:1) as a solvent in a Soxhlet apparatus for 16 h. After asphaltenes were precipitated with *n*-hexane, extracts and whole oils were fractionated using alumina silica gel column chromatography into aliphatic hydrocarbons, aromatic hydrocarbons, and polar fractions with *n*-hexane, toluene, and toluene/methanol, respectively.

The American Petroleum Institute (API) gravity and elemental analyses such as sulfur, nickel, and vanadium of crude oils were analyzed utilizing Rudolph DDM2911 Density Meter, Thermo Fisher Scientific® ASTM D4294, and a PerkinElmer® ASTM D5863, respectively.

Saturated and aromatic hydrocarbon fractions stable carbon isotopic compositions ($\delta^{13}\text{C}$) of source rock extracts and oils were determined using methods described by Sofer (1980). The stable carbon isotope analysis was carried out using a DELTA V™ Isotope Ratio mass spectrometer (IRMS), with



◀ **Fig. 4.** Summary stratigraphy of the central Gulf of Suez (modified after Alsharhan and Salah 1995; Bosworth et al. 2014).

± 0.02‰ analytical precision based on the Pee Dee Belemnite standard.

Saturate and aromatic fractions of oils and extracts were analyzed using gas chromatography (GC) and full-scan gas chromatography–mass spectrometry (GC–MS). Saturate fractions were analyzed using a Hewlett-Packard® 5890 equipped with a 30 m × 0.25 mm ID × 0.25 μm film thickness HP-5MS fused silica capillary column. N₂ was used as the carrier gas at a flow rate of 1.5 ml/min, and the samples were injected in a splitless mode maintained at 300 °C. The GC oven temperature was programmed from 50° to 300 °C at 3 °C/min, with a final hold at 300 °C for 30 min. Samples were routinely analyzed in full-scan mode using selective ion monitoring (SIM) mode.

Quantitative and qualitative GC–MS analyses completed on crude oils and rock extracts were performed using a Hewlett-Packard® 6890 GC/5973 MSD equipped with a HP-5MS column (30 m × 0.25 mm ID × 0.25 μm film thickness). The mass spectrometer was operated with electron ionization energy at 70 eV, and He was the carrier gas. The GC oven temperature was initially set at 50 °C, programmed to 120 °C at 20 °C/min, to 250 °C at 4 °C/min, then to 310 °C at 3 °C/min with a final hold of 30 °C min. Biomarker parameters were calculated from base peak responses at *m/z* 71 for *n*-alkanes, *m/z* 217 for steranes, *m/z* 191 for terpanes, *m/z* 231 for triaromatic steroids, *m/z* 253 for monoaromatic steroids, *m/z* 178 + 192 for phenanthrene and methylphenanthrene, and *m/z* 184 + 198 dibenzothiophenes and methyl dibenzothiophene.

In some cases, limited sample size prevented API, S, or δ¹³C analyses or allowed only a single analysis. All geochemical analyses presented herein were done at the Department of Applied Geosciences and Geophysics, Montanuniversität Leoben, Austria, the GeoMark Research, Ltd. Texas, and StratoChem Services, Cairo.

The chemometric decision tree method (Peters et al. 2007; El Diasty et al. 2016, 2017a) of selected source-related biomarker ratios (see oil chemometric section for the selected parameters) was applied using Pirouette® 4.5 software (Infometrix Inc., Bothell, Washington). Two exploratory algorithms in Pirouette include HCA and PCA. HCA categorizes samples into genetic families based on the distance

between samples in *n*-space where *n* represents the measured independent variables. PCA is a more rigorous correlation tool that reduces the dimensionality of the data to a few principal components (eigenvectors) that quantify the distance between samples in principal component space. An HCA dendrogram showing the cluster distances between samples was built using incremental linkage and Euclidean metric distance. Auto-scale preprocessing of the independent variables was used for both HCA and PCA. Auto-scaling ensures that each variable has equal weight in the determination of genetic affinities among samples.

InStep™ is automated chemometrics software that can be used to build an effective model for classification of new samples using a decision tree based on multivariate classification of a previously analyzed training set. The training set for this study consisted of 46 oil samples classified into six families using Pirouette 4.5™ software based on 16 source-related biomarker ratios. InStep takes the Pirouette results to create a multivariate model that predicts each classification for new samples, such as the 39 rock extract samples in this study. This requires that the input rock extract data consist of the same 16 source-related biomarker ratios in the same order as that used to classify the oil samples. The decision tree in this study was constructed using soft independent modeling of class analogy (SIMCA). SIMCA makes a separate PCA model for each of the six families and gives diagnostics to show how the classes differ from each other. For SIMCA, we used auto-scale preprocessing with two factors and a probability threshold of 0.9500. The fit of the extracts to the oil families is described as “good” at the 95% confidence (2 sigma) or fair at 99% confidence (3 sigma). Samples that do not fit a family (“not classified”) have confidence levels > 99%. InStep uses a “watched folder” approach for sample handling, i.e., whenever a data file with the appropriate format is delivered, InStep processes the samples in the file and generates a report in the watched folder.

RESULTS AND DISCUSSION

Source Rock Geochemistry

Screening Analyses: TOC and Rock-Eval Pyrolysis

Table 1 compares TOC and Rock-Eval data for the Upper Cretaceous–Eocene or pre-Miocene

Table 1. The abundance of organic matter in source rocks from the Gulf of Suez Rift basin

No.	Field	Depth (m)	Formation	TOC (wt%)	S ₂	S ₃	T _{max} (°C)	Calc. R _o	HI	OI	PI	S ₂ /S ₃
1	Geisum	482	Belayim	2.28	8.21	2.8	428	0.54	360	123	0.08	2.93
2	October	1996	Belayim	1.21	4.12	1.15	428	0.54	340	95	0.06	3.58
3	October	2027	Belayim	1.08	3.65	0.98	432	0.62	338	91	0.06	3.72
4	October	2134	Belayim	1.18	2.23	1.07	431	0.60	189	91	0.09	2.08
5	Belayim Marine	2200	Belayim	1.37	1.95	3.60	425	0.49	142	263	0.01	0.54
6	Belayim Marine	2260	Belayim	1.62	3.76	4.86	425	0.49	232	300	0	0.77
7	Belayim Marine	2310	Belayim	2.45	7.72	4.09	422	0.44	315	167	0.02	1.89
8	SB 276	2579	Belayim	1.77	6.8	5.47	428	0.54	384	309	0.01	1.24
9	SB 276	2596	Belayim	1.81	6.97	4.71	435	0.67	385	260	0.03	1.48
10	North Shadwan	3347	Rudeis	1.39	4.59	2.04	430	0.58	330	147	0.08	2.25
11	Belayim Land	4050	Rudeis	8.45	23.84	2.33	437	0.71	282	28	0.81	10.23
12	Amal	2499	Rudeis	1.53	3.73	2.83	431	0.60	244	185	0	1.32
13	Amal	2398	Rudeis	1.55	2.84	0.90	430	0.58	183	58	0.02	3.16
14	Amal	2471	Rudeis	1.57	3.38	3.08	432	0.62	215	196	0.11	1.10
15	Amal	2499	Rudeis	1.53	3.73	2.83	431	0.60	244	185	0	1.32
16	Geisum	1972	Rudeis	1.33	2.07	0.76	429	0.56	156	57	0.02	2.74
17	Morgan	2225	Rudeis	2.14	4.86	1.43	433	0.63	227	67	0.06	3.39
18	Morgan	2252	Rudeis	2.29	4.97	1.03	434	0.65	217	45	0.05	4.82
19	Morgan	2475	Rudeis	1.81	3.29	0.83	433	0.63	182	46	0.06	3.96
20	Morgan	2408	Rudeis	3.34	12.33	1.58	434	0.65	369	47	0.79	7.80
21	Belayim Marine	3139	Rudeis	1.11	2.84	1.01	431	0.60	256	91	0.04	2.81
22	Belayim Marine	3151	Rudeis	1.82	9.25	0.98	438	0.72	508	54	0.01	9.41
23	Belayim Marine	3159	Rudeis	1.94	8.19	1.07	440	0.76	422	55	0.02	7.67
24	Belayim Marine	3181	Rudeis	1.97	10.2	0.59	438	0.72	518	30	0.02	17.27
25	Belayim Marine	3202	Rudeis	1.42	5.08	1.31	443	0.81	358	92	0.02	3.89
26	Belayim Marine	3220	Rudeis	1.41	6.91	1.24	441	0.78	490	88	0.02	5.57
27	Belayim Marine	3232	Rudeis	1.29	7.15	0.65	414	0.29	554	50	0.02	11.08
28	Belayim Marine	3250	Rudeis	1.63	6.94	0.29	441	0.78	426	18	0.01	23.67
29	Belayim Marine	3256	Rudeis	1.76	6.11	0.35	443	0.81	347	20	0.03	17.35
30	October	2576	Rudeis	1.00	2.50	0.74	439	0.74	250	74	0.10	3.38
31	October	2621	Rudeis	0.88	3.33	0.69	435	0.67	378	78	0.07	4.83
32	October	2712	Rudeis	0.94	1.78	0.73	433	0.63	198	78	0.19	2.44
33	October	2819	Rudeis	1.14	4.62	1.01	440	0.76	405	89	0.10	4.57
34	October	2910	Rudeis	1.00	2.57	0.67	434	0.65	257	67	0.09	3.84
35	October	3155	Rudeis	0.84	2.29	0.35	437	0.71	273	42	0.08	6.54
36	October	3048	Rudeis	0.89	3.91	0.81	435	0.67	439	91	0.13	4.83
37	October	3109	Rudeis	0.85	2.40	0.40	435	0.67	328	47	0.10	6.00
38	October	3139	Rudeis	0.82	2.61	0.51	440	0.76	318	621	0.09	5.12
39	October	3155	Rudeis	0.84	2.29	0.35	437	0.71	273	42	0.08	6.54
40	October	3185	Rudeis	0.81	2.78	0.54	439	0.74	343	67	0.09	5.15
41	October	3200	Rudeis	0.96	3.57	0.53	439	0.74	372	55	0.07	6.74
42	October	3216	Rudeis	0.99	3.19	0.37	435	0.67	322	37	0.06	8.62
43	October	3231	Rudeis	1.06	4.37	0.96	441	0.78	412	91	0.07	4.55
44	October	3246	Rudeis	0.87	2.91	0.79	441	0.78	334	91	0.07	3.68
45	October	3237	Rudeis	1.92	5.15	1.32	435	0.67	268	69	0.08	3.88
46	October	3337	Rudeis	1.67	4.58	0.89	436	0.69	274	53	0.07	5.17
47	October	3392	Rudeis	1.61	4.01	0.53	441	0.78	249	33	0.02	7.55
48	North Shadwan	3347	Rudeis	1.39	4.59	2.04	430	0.58	330	147	0.08	2.25
49	Ras Ghara	2010	Nukhul	1.32	3.41	0.66	428	0.54	258	50	0.16	5.17
50	Ras Ghara	2016	Nukhul	0.62	1.45	0.43	427	0.53	234	69	0.26	3.37
51	Ras Ghara	2169	Nukhul	0.39	0.82	0.46	426	0.51	209	117	0.36	1.78
52	Geisum	2316	Nukhul	2.18	9.13	1.09	435	0.67	419	50	0.01	8.38
53	Geisum	2335	Nukhul	2.50	12.03	0.88	433	0.63	481	35	0	13.74
54	Geisum	2390	Nukhul	2.23	9.41	1.29	434	0.65	422	58	0.01	7.28
55	Geisum	2490	Nukhul	2.43	11.15	1.63	436	0.69	459	67	0.01	6.85
56	Geisum	2536	Nukhul	1.99	8.58	0.76	433	0.63	431	38	0	11.34
57	October	3307	Nukhul	0.61	2.53	0.88	447	0.89	415	144	0.09	2.88
58	SB 276	3767	Nukhul	1.77	8.04	0.58	435	0.67	454	33	0.04	13.76

Table 1. continued

No.	Field	Depth (m)	Formation	TOC (wt%)	S ₂	S ₃	T _{max} (°C)	Calc. R _o	HI	OI	PI	S ₂ /S ₃
59	Belayim Marine	2858	Thebes	2.83	13.70	3.42	427	0.53	484	121	0.04	4.00
60	Belayim Marine	2902	Thebes	2.40	13.70	1.97	429	0.56	571	82	0.11	6.96
61	Belayim Marine	2920	Thebes	1.85	9.82	1.87	429	0.56	531	101	0.10	5.26
62	Belayim Marine	2978	Thebes	2.72	13.82	2.23	426	0.51	508	82	0.06	6.20
63	Belayim Marine	3202	Thebes	5.18	33.15	0.41	436	0.69	640	8	0.42	80.00
64	Belayim Marine	3204	Thebes	5.72	50.16	0.34	434	0.65	877	6	0.30	146.17
65	Belayim Marine	3207	Thebes	4.75	39.24	0.38	437	0.71	826	8	0.27	103.25
66	Belayim Marine	3209	Thebes	5.63	48.42	0.34	438	0.72	860	6	0.30	143.33
67	Belayim Marine	3216	Thebes	4.42	34.08	0.35	437	0.71	771	8	0.39	96.38
68	SB 276	3892	Thebes	1.60	7.90	0.80	434	0.65	494	50	0.02	9.88
69	Amer	841	Thebes	2.31	8.71	1.78	426	0.51	377	77	0.07	4.90
70	Amer	886	Thebes	3.75	22.65	1.50	433	0.63	604	40	0.13	15.10
71	Amer	933	Thebes	3.36	23.62	1.21	429	0.56	703	36	0.06	19.53
72	Amer	987	Thebes	2.77	13.66	2.60	441	0.78	493	94	0.09	5.24
73	Amal	2703	Thebes	2.00	5.78	2.66	434	0.65	289	133	0.13	2.17
74	Morgan	3094	Thebes	1.85	9.82	1.87	429	0.56	531	101	0.10	5.26
75	July	3509	Thebes	2.72	13.82	2.23	426	0.51	508	82	0.06	6.20
76	October	3179	Thebes	2.73	9.47	2.43	435	0.67	347	89	0.26	3.90
77	Geisum	2563	Esna	2.03	8.16	1.08	434	0.65	402	53	0.01	7.58
78	Geisum	2627	Esna	2.32	8.65	2.39	433	0.63	373	103	0.25	3.62
79	Belayim Marine	3259	Esna	2.63	11.26	0.84	439	0.74	428	32	0.01	13.38
80	Belayim Marine	3265	Esna	2.25	8.57	0.97	442	0.80	381	43	0.03	8.86
81	Belayim Marine	3274	Esna	3.38	11.42	1.28	443	0.81	338	38	0.02	8.89
82	Belayim Marine	3277	Esna	2.72	9.03	0.95	432	0.62	332	35	0.02	9.49
83	Amer	1021	Esna	2.20	8.76	2.44	433	0.63	398	111	0.02	3.59
84	Amal	2749	Esna	4.12	15.61	2.47	432	0.62	379	60	0.10	6.32
85	October	3249	Esna	1.95	6.28	0.90	433	0.63	322	46	0.11	7.00
86	October	3383	Esna	1.13	4.13	1.54	440	0.76	365	136	0.07	2.67
87	October	3398	Esna	1.96	8.28	1.60	440	0.76	422	82	0.04	5.17
88	Belayim Land	4722	Br. LS	5.05	20.28	1.29	435	0.67	402	26	0.71	15.72
89	October	3590	Br. LS	2.13	10.66	1.23	428	0.54	500	58	0.28	8.67
90	July	3566	Br. LS	4.48	13.93	0.88	437	0.71	311	20	0.83	15.83
91	Amal	2804	Br. LS	2.55	8.13	5.41	434	0.65	319	212	0.12	1.5
92	Ghara	2208	Br. LS	4.43	24.53	1.34	417	0.35	554	30	0.08	18.31
93	Geisum	2655	Br. LS	3.02	11.96	2.87	430	0.58	396	95	0.01	4.17
94	Geisum	2673	Br. LS	3.15	11.47	3.37	431	0.60	364	107	0.24	3.40
95	Geisum	2691	Br. LS	3.60	16.52	2.56	432	0.62	459	71	0	6.46
96	Geisum	2700	Br. LS	1.80	6.14	2.56	437	0.71	341	142	0.3	2.40
97	Geisum	2719	Br. LS	2.41	8.00	1.21	431	0.60	332	50	0.12	6.64
98	Belayim Marine	3114	Br. LS	5.26	33.87	2.68	426	0.51	644	51	0.05	12.63
99	Belayim Marine	3134	Br. LS	3.80	23.48	1.48	431	0.60	618	39	0.04	15.85
100	Belayim Marine	3144	Br. LS	2.69	14.34	2.13	429	0.56	533	79	0.05	6.75
101	North Shadwan	3669	Br. LS	2.40	9.76	1.19	433	0.63	407	50	0.24	8.20
102	SB 276	4084	Br. LS	3.37	12.91	0.94	439	0.74	383	28	0.06	13.68
103	Amer	1088	Br. LS	2.58	8.39	1.68	425	0.49	325	65	0.01	5.00
104	Amer	1106	Br. LS	2.76	10.32	2.13	425	0.49	374	77	0.01	4.86
105	Amer	1124	Br. LS	3.05	14.95	2.32	423	0.45	490	76	0.05	6.45
106	Amer	1149	Br. LS	2.66	9.23	4.81	423	0.45	347	181	0.05	1.92
107	Morgan	2813	Br. LS	8.11	46.23	1.38	428	0.54	570	17	0.02	33.53
108	Morgan	2831	Br. LS	2.27	11.28	2.54	429	0.56	497	112	0	4.44
109	Morgan	2843	Br. LS	3.60	19.58	2.20	422	0.44	544	61	0.12	8.92
110	Morgan	3164	Br. LS	6.91	34.76	2.83	431	0.60	503	41	0.64	12.28
111	October	3414	Br. LS	2.66	15.66	1.20	442	0.80	589	45	0.02	13.05
112	North Shadwan	3749	Matulla	2.52	11.08	4.50	436	0.69	440	179	0.17	2.46
113	Amal	2849	Matulla	2.15	2.43	0.86	440	0.76	113	40	0.04	2.83
114	Geisum	2801	Matulla	2.81	4.66	0.87	439	0.74	166	31	0.11	5.35
115	Belayim Marine	3372	Matulla	0.90	1.86	1.07	431	0.60	207	119	0.04	1.74
116	Belayim Marine	3912	Matulla	1.25	1.68	1.16	436	0.69	134	93	0.07	1.45

Table 1. continued

No.	Field	Depth (m)	Formation	TOC (wt%)	S ₂	S ₃	T _{max} (°C)	Calc. R _o	HI	OI	PI	S ₂ /S ₃
117	Belayim Marine	3942	Matulla	0.76	0.88	1.16	435	0.67	116	157	0.12	0.76
118	October	3490	Matulla	0.64	0.91	0.40	440	0.76	142	69	0.17	2.07
119	October	3520	Matulla	0.82	0.84	0.76	440	0.76	102	93	0.23	1.11
120	October	3536	Matulla	0.76	1.62	0.74	446	0.87	213	97	0.15	2.19
121	October	3636	Matulla	1.11	1.31	3.07	433	0.63	118	277	0.31	0.43
122	October	3718	Matulla	1.30	1.04	1.04	433	0.63	80	80	0.17	1.00
123	SB 276	4124	Matulla	2.43	2.21	2.38	439	0.74	91	98	0.05	0.93

TOC, total organic carbon (wt%); S₂, hydrocarbons from kerogen cracking (mg HC/g rock); S₃, organic CO₂—kerogen derived (mg CO₂/g rock); T_{max}, pyrolysis temperature at which maximum emission of hydrocarbons occurs (°C); Calc. R_o, calculated R_o = 0.0180 × T_{max} - 7.16; HI, hydrogen index = S₂ × 100/TOC, OI, oxygen index = S₃ × 100/TOC; PI, production index = S₁/S₁ + S₂

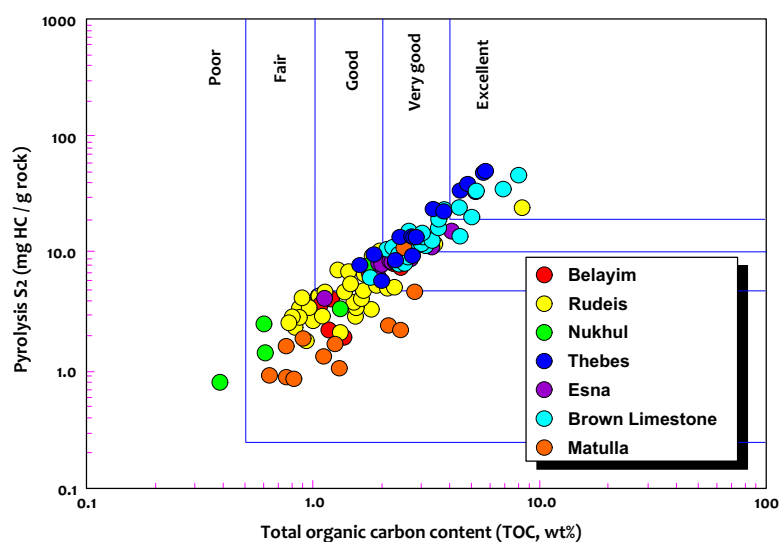


Fig. 5. Plot of total organic carbon (TOC, wt%) versus pyrolysis S₂ (mg HC/g rock) results for rock samples from the Gulf of Suez, showing source rock quality classifications. TOC content varies substantially among the rock samples. Organic-rich intervals occur in the Campanian Brown Limestone and the Eocene Thebes samples with very good-to-excellent quantities of organic matter.

(Matulla, Brown Limestone, Esna, and Thebes) and Lower–Middle Miocene (Nukhul, Rudeis and Belayim) samples. TOC content of the studied rock units varies substantially between 0.39 and 8.45 wt% with an average 2.38 wt%. The organic-rich intervals occur in the Campanian Brown Limestone ($n = 24$, 1.8–8.11 wt%, average 3.64 wt%), and the Thebes samples ($n = 18$, 1.6–5.72 wt%, average 3.29 wt%). Therefore, pre-Miocene source units (Brown Limestone and Thebes samples) contain very good-to-excellent quantities of organic matter (Fig. 5). High TOC contents are directly linked to

low oxygenation of the water column, the dominant redox conditions of the bottom sediments (El Diasty et al. 2014, 2017b), and the high productivity upwelling regime that existed during Late Cretaceous–Early Paleogene time (Robinson and Engel 1993; El-Shafeiy et al. 2017). The richness of the Brown Limestone and Thebes Formation is also confirmed by pyrolysis yields (S₂). The pre-Miocene is rated very good to excellent, whereas the Miocene is rated fair to good where the sedimentary environment possibly was less favorable for preservation of organic material.

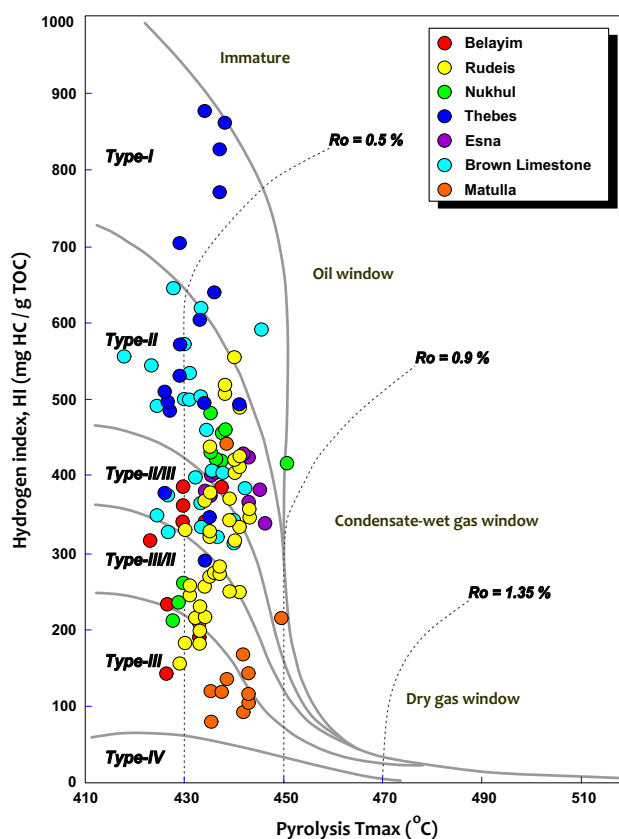


Fig. 6. Plot of pyrolysis T_{\max} versus hydrogen index (HI) shows that the analyzed samples contain variable kerogen types (mainly Type II and Type II/III kerogen) and correspond mostly immature to peak oil window (see Peters and Cassa 1994; Mukhopadhyay et al. 1995).

The Rock-Eval pyrolysis is a simple, inexpensive and rapid screening technique for information on source rock potential (Espitalié et al. 1985; Lafargue et al. 1998). Kerogen quality and maturity are usually determined by plotting hydrogen index (HI, mg HC/g TOC) against T_{\max} (pyrolysis S_2 peak temperature) rather than HI (Fig. 6) versus oxygen index (OI, mg HC/g CO_2). Thus, many kerogen-type designations are based on the HI to avoid the use of OI (Tissot and Welte 1984; Espitalié et al. 1985; Mukhopadhyay et al. 1995). Figure 6, showing HI and T_{\max} data, indicates variable kerogen type and maturation histories in different parts of the Suez Rift, which are related to differences in organic facies, paleo-heat flow, and lithology-related heat conductivity and heat capacity (Cornford et al. 1998;

Dembicki 2009). Most of the analyzed samples lie in the Type II and Type II/III maturation paths with a few samples falling within the kerogen Type I or Type III pathways. The source rock potential based on Rock-Eval pyrolysis falls between two end-members: the Upper Cretaceous Matulla Formation samples (Type III gas-prone source rocks) and the Eocene Thebes Formation samples (Type I oil-prone source rocks). When the organic matter in a source rock starts to generate hydrocarbons due to thermal stress, the transformation of kerogen into hydrocarbons modifies original organic matter characteristics (HI, S_2 , TOC) and thus complicates interpretations and implications about the original quantity and quality of the organic matter (Hunt 1996; Dembicki 2009; Carvajal-Ortiz and Gentzis 2015).

Table 2. Geologic, stable carbon isotopic, and gas chromatographic data for source rocks from the Gulf of Suez Rift basin

No.	Field	Well name	Depth (m)	Type	Age	Formation	Lithology	Ph/n-C ₁₈	Pr/n-C ₁₇	Pr/Ph	CPI	$\delta^{13}\text{C}_{\text{Sat}}$	$\delta^{13}\text{C}_{\text{Aro}}$	CV
1	Geisum	Geisum	1210	Cutting	M. Miocene	Belayim	Shale	0.30	0.60	0.50				
2	Amal	Amal	1862	Cutting	M. Miocene	Belayim	Shale	0.30	0.60	0.40	1.0			
3	Morgan	Morgan	2408	Cutting	L. Miocene	Rudeis	Shale	0.56	0.53	0.97	1.25	-28.1	-27.2	-0.94
4	North Shadwan	North Shadwan-1	3347	Cutting	L. Miocene	Rudeis	Shale	0.72	1.05	1.67	1.11	-26.5	-24.1	1.89
5	Ras Ghara	Ras Ghara-1	3400	Cutting	L. Miocene	Rudeis	Shale	0.47	0.43	0.79		-27.4	-26.4	-0.94
6	Ras Ghara	Ras Ghara-2	3415	Cutting	L. Miocene	Rudeis	Shale	0.48	0.44	0.85		-29.3	-27.7	0.98
7	Ras Ghara	Ras Ghara-3	3465	Cutting	L. Miocene	Rudeis	Calc. Shale	0.52	0.48	0.76		-28.1	-26.8	-0.05
8	Ras Ghara	Ras Ghara-3	3520	Cutting	L. Miocene	Rudeis	Calc. Shale	0.50	0.47	0.67				
9	Belayim Land	Belayim Land	4050	Cutting	L. Miocene	Rudeis	Shale	0.47	0.45	0.92	1.15	-27.9	-26.9	-0.78
10	Ras Ghara	Ras Ghara-4	2010	Cutting	L. Miocene	Nukhul	Shale	0.44	0.33	0.49	0.99			
11	Ras Ghara	Ras Ghara-4	2016	Cutting	L. Miocene	Nukhul	Shale	0.50	0.35	0.48	1.01			
12	Ras Ghara	Ras Ghara-4	2169	Cutting	L. Miocene	Nukhul	Limestone	0.55	0.43	0.47	1.0			
13	Geisum	Geisum	2316	Cutting	L. Miocene	Nukhul	Shale	0.80	0.90	1.30		-30.3	-30.3	-2.26
14	Ras Ghara	Ras Ghara-3	3615	Cutting	L. Miocene	Nukhul	Shale	0.51	0.49	0.67		-27.6	-28.2	-4.43
15	Amer	Amer	948	Cutting	Eocene	Thebes	Limestone	1.50	1.10	0.60	1.0	-28.5	-27.8	-1.26
16	Amal	Amal	2716	Cutting	Eocene	Thebes	Limestone	0.60	0.50	0.70	1.0	-28.2	-27.4	-1.13
17	Sinai	Sinai	3090	Cutting	Eocene	Thebes	Limestone	0.51	0.45	0.30		-28.4	-27.4	-0.63
18	Morgan	Morgan	3094	Cutting	Eocene	Thebes	Limestone	0.55	0.54	1.07	1.15	-28.1	-27	-0.50
19	October	October-A	3139	Cutting	Eocene	Thebes	Limestone	0.80	0.60	0.8	1.0			
20	Belayim Marine	Belayim Marine	3210	Core	Eocene	Thebes	Limestone	0.56	0.39	0.56				
21	Belayim Marine	Belayim Marine	3216	Core	Eocene	Thebes	Limestone	0.68	0.42	0.68				
22	July	July	3502	Cutting	Eocene	Thebes	Limestone	0.53	0.50	0.94	1.1	-28.4	-27.4	-0.63
23	SB 276	SB 276	3871	Cutting	Eocene	Thebes	Limestone	0.60	0.40	0.50	1.0			
24	Geisum	Geisum	2560	Cutting	Paleocene	Esna	Shale	0.70	1.10	0.70	0.9	-28.2	-27.2	-0.69
25	Sinai	Sinai	3100	Cutting	Paleocene	Esna	Shale	0.49	0.49	0.91		-28.9	-27.2	1.08
26	Amer	Amer	1149	Cutting	Campanian	Br. LS	Limestone	0.70	0.80	1.00		-28.2	-27.8	-2.02
27	Ras Ghara	Ras Ghara-4	2208	Cutting	Campanian	Br. LS	Limestone	0.38	0.28	0.69	1.02			
28	Geisum	Geisum	2682	Cutting	Campanian	Br. LS	Limestone	0.50	0.40	0.90	1.00	-28.5	-27.8	-1.26
29	Amal	Amal	2807	Cutting	Campanian	Br. LS	Limestone	0.50	0.30	0.70	1.00	-29.2	-28.7	-1.49
30	Sinai	Sinai	3120	Cutting	Campanian	Br. LS	Argil. LS	0.54	0.46	0.78		-29.2	-29.3	-2.82
31	October	October-A	3554	Cutting	Campanian	Br. LS	Argil. LS	0.90	0.70	0.60	0.90	-28.9	-28.3	-1.36
32	July	July	3566	Cutting	Campanian	Br. LS	Limestone	0.50	0.46	0.97	1.17	-28.3	-27.3	-0.66
33	October	October-B	3590	Cutting	Campanian	Br. LS	Limestone	0.57	0.53	1.23	0.94	-28.6	-28.0	-1.45
34	North Shadwan	North Shadwan-2	3669	Cutting	Campanian	Br. LS	Limestone	0.42	0.25	0.57	0.91	-29.6	-29.5	-2.25
35	SB 276	SB 276	4081	Cutting	Campanian	Br. LS	Limestone	0.80	1.00	1.20	0.90			
36	Belayim Land	Belayim Land	4722	Cutting	Campanian	Br. LS	Limestone	0.46	0.42	0.91	1.07	-28.2	-26.9	-0.02
37	Sinai	Sinai	3180	Cutting	Coniacian	Matulla	Calc. Shale	0.45	0.60	1.55		-27.2	-25.5	0.56
38	North Shadwan	North Shadwan-2	3749	Cutting	Coniacian	Matulla	Calc. Shale	0.44	0.40	0.83	0.83	-29.0	-27.9	-0.22
39	SB 276	SB 276	4124	Cutting	Coniacian	Matulla	Limestone	0.60	0.60	0.90	1.20			

Ph/n-C₁₈, phytane/n-octadecane; Pr/n-C₁₇, pristane/n-heptadecane; Pr/Ph, pristane/phytane; CPI, carbon preference index = [(C₂₅ + C₂₇ + C₂₉ + C₃₁ + C₃₃)/(C₂₆ + C₂₈ + C₃₀ + C₃₂ + C₃₄) + (C₂₅ + C₂₇ + C₂₉ + C₃₁ + C₃₃)/(C₂₄ + C₂₆ + C₂₈ + C₃₀ + C₃₂)]/2; $\delta^{13}\text{C}_{\text{Sat}}$ & $\delta^{13}\text{C}_{\text{Aro}}$, saturated and aromatic hydrocarbons stable carbon isotope; CV, canonical variable = $-2.53\delta^{13}\text{C}_{\text{Sat}} + 2.22\delta^{13}\text{C}_{\text{Aro}} - 11.65$

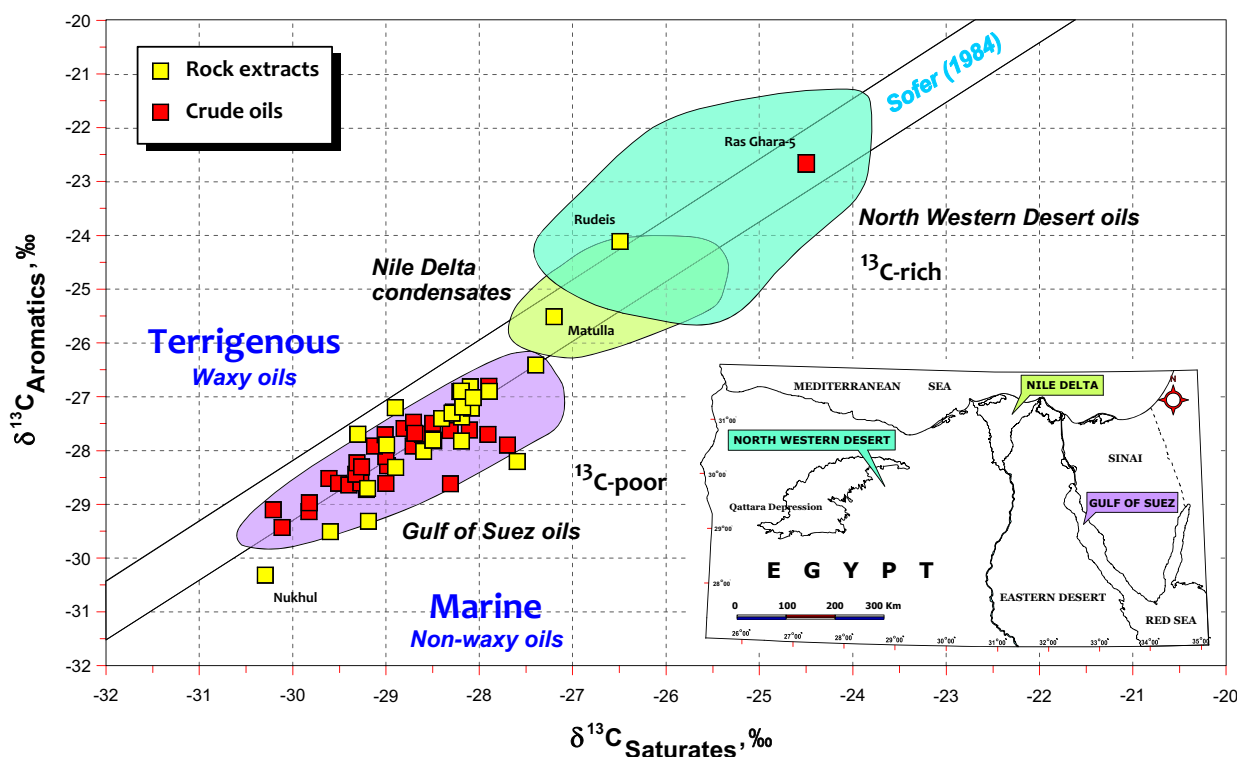


Fig. 7. Isotope composition of saturated versus aromatic hydrocarbon fractions for the extracted bitumen and crude oil samples from the Gulf of Suez to illustrate isotopic differences between waxy and marine oils. The two diagonal lines are the best fit for terrigenous (top) and marine (bottom) oil samples from Sofer (1984).

Stable Carbon Isotope Composition

Stable carbon isotope results ($\delta^{13}\text{C}$, ‰) for the saturated and aromatic hydrocarbon fractions from the source rock extracts are listed in Table 2. Carbon isotope values indicate that most of the samples have $\delta^{13}\text{C}$ values ranging from -29.5 to -27.5 ‰ and -29.0 to -27.0 ‰ (Fig. 7) for the alkanes and aromatics, respectively. These values are indicative of predominantly marine-derived organic matter with minor terrigenous input (Collister and Wavrek 1996; El Diasty et al. 2018). Slightly less negative (more positive) values have been recorded for the Rudeis (sample no. 4, -26.5 to -24.1 ‰, for the saturates and aromatics, respectively) and Matulla (sample no. 13, -27.2 to -25.5 ‰, for the saturates and aromatics, respectively) from the North Shadwan and Geisum oilfields in the southern sector of the Gulf of Suez basin, suggesting a mixture of terrigenous- and marine-derived organic matter in the source rock (Sofer 1984).

Applying the method adopted by Sofer (1984) to distinguish between oils generated from terrige-

nous and marine sources suggests that the extracts contain predominantly marine-derived organic matter, typical of Gulf of Suez oils (Fig. 7).

Normal Alkanes and Acyclic Isoprenoids

Figure 8 shows gas chromatograms of saturated hydrocarbons for representative source rock extract samples from the Gulf of Suez Province. The results of these analyses are summarized in Table 2. The most prominent features that most extracts share include: (1) the unimodal low molecular weight skewed *n*-alkane distribution; (2) the absence of evidence for biodegradation; (3) low concentrations of *n*-alkanes $>C_{23}$, with common maxima between *n*- C_{17} and *n*- C_{20} ; and (4) lack of odd-over-even predominance or carbon preference index (CPI) where most values are around unity, exceptions may occur in some samples (Table 2). These common characteristics, in addition to acyclic C_{19} and C_{20} isoprenoids [2-, 6-, 10-, 14-tetramethylpentadecane or pristane (Pr) and 2-, 6-, 10-, 14-tetramethylhexade-

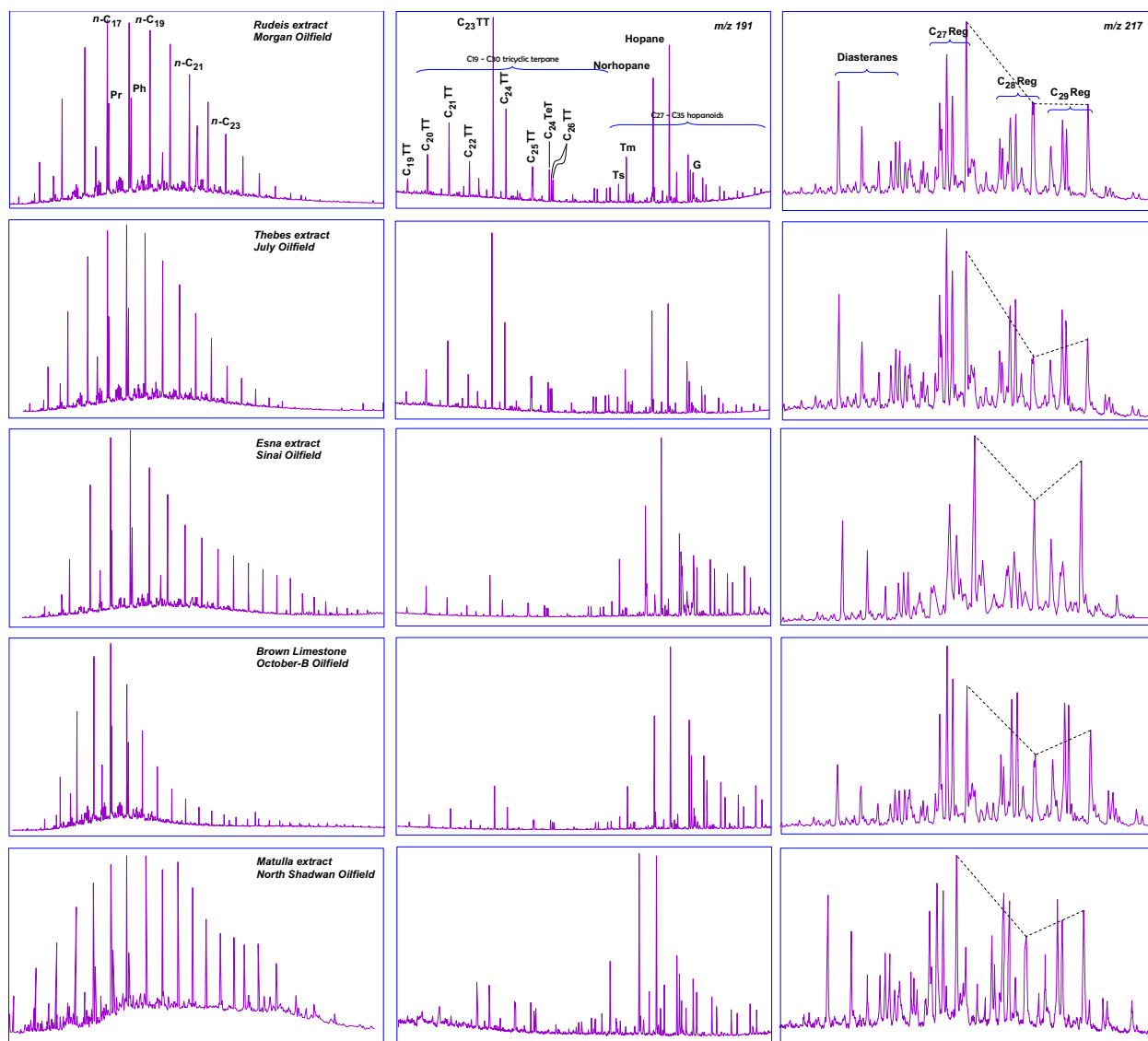


Fig. 8. Gas chromatography and gas chromatography–mass spectrometry (GC–MS) show the distributions of normal alkanes and isoprenoids, terpanes (m/z 191) and steranes (m/z 217) mass fragmentograms of saturated hydrocarbons for representative extract samples in this study.

cane or phytane (Ph)], indicate hypersaline or carbonate environments and anoxic conditions with substantial algal/bacterial organic matter (Didyk et al. 1978; Peters et al. 2005). Ph is present in relatively high concentrations compared to Pr, where Pr/Ph in most cases < 0.8 (average). The high abundance of Ph and low Pr/Ph ratios for these sediments may have resulted from the presence of halophilic bacteria that contain complex lipids with a phytanyl moiety (ten Haven et al. 1987) and relatively high amounts of organic sulfur in these marine sediments (Sinninghe Damsté et al. 1989). Excep-

tions may occur in some samples (no. 4, 13, 18, 26, 33, 35, and 37) where Pr/Ph > 1.0 , which indicates the presence of a mixture of terrigenous- and algal-derived organic matter deposited in mildly reducing conditions (Mostafa 1993).

Isoprenoids/ n -paraffin ratios, expressed by Pr/ n -C₁₇ and Ph/ n -C₁₈ (Table 2), are often used to provide information on source, maturation, and biodegradation (Connan and Cassou 1980; Peters et al. 1999). In this study, Pr and Ph occur in a moderate abundance relative to n -alkanes resulting in average Pr/ n -C₁₇ and Ph/ n -C₁₈ values of 0.54 and

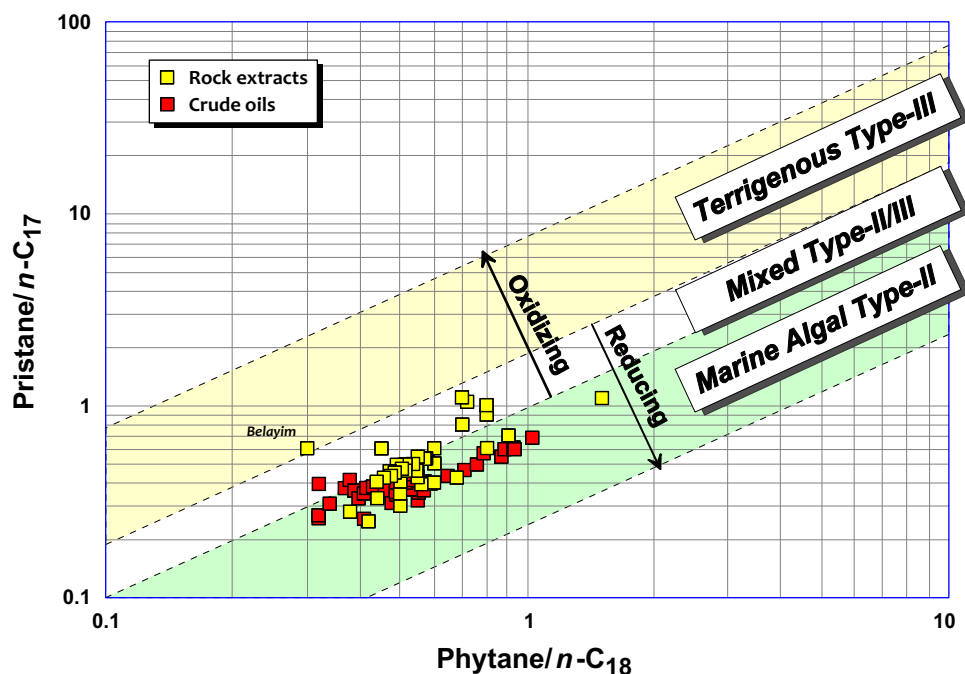


Fig. 9. Plot of $Ph/n-C_{18}$ versus $Pr/n-C_{17}$ from gas chromatograms indicates either marine algal Type II or mixed Type II/III kerogens deposited under anoxic conditions for the Gulf of Suez oil and sediments (see Peters et al. 1999).

0.57, respectively. The input of terrigenous materials was only minor, except two extract samples from the Belayim Formation, and the organic material can be classified as a mixture of an oil-prone Type II and -II/III kerogens (Fig. 9).

Terpanes and Steranes

Biomarkers are important geochemical tools (Fig. 8; Table 3). For example, terpanes (m/z 191) and steranes (m/z 217) yield very specific information on source, biodegradation, maturation, and migration of crude oil and related source rocks (Trendel et al. 1982; Tissot and Welte 1984; Peters et al. 2005; El Diasty et al. 2017b).

The extracted bitumen samples from different stratigraphic units and fields in the Gulf of Suez show widely variable terpane and sterane distributions (Table 3). Most of the analyzed samples have low concentrations of tricyclic and tetracyclic terpanes relative to pentacyclic terpanes (Fig. 8). Interestingly, samples from the Thebes and Belayim extracts show very high abundance of tricyclic terpanes with a maximum C_{23} tricyclic terpane. The tricyclic terpenoids or cheilanthanes are likely de-

rived from specific bacterial membrane lipids and are characteristic of marine source (Aquino Neto et al. 1983; Ourisson et al. 1984; Peters et al. 2005).

Several distinct biomarker ratios (Fig. 8; Table 3) are useful to describe the analyzed sediments from the Gulf of Suez. These include C_{19}/C_{23} , C_{23}/C_{24} , and C_{25}/C_{26} tricyclic terpanes, C_{24} tetracyclic/ C_{26} tricyclic terpanes, C_{27} $18\alpha(H)$ -trisorneohopane (Ts)/ C_{27} $17\alpha(H)$ -trisorhopane (Tm), C_{35}/C_{34} homohopanes, oleanane/hopane, and gammacerane/hopane (Seifert and Moldowan 1978; Kolaczowska et al. 1990; Moldowan et al. 1991; Sinninghe Damsté et al. 1995).

The Gulf of Suez sediments consist of shale/marl and carbonate source rocks that contain algal/bacterial organic matter with little higher-plant input, based on very low C_{19}/C_{23} , high C_{23}/C_{24} , and C_{25}/C_{26} tricyclic terpanes, and the relatively high C_{24} tetracyclic/ C_{26} tricyclic terpane ratios (Table 3). The presence of norhopane as indicated by the peak C_{29} $17\alpha(H)$ -hopane in appreciable amounts over C_{30} $17\alpha(H)$ -hopane in some Matulla and Thebes extracts indicates clay-poor carbonate/marl or evaporite source depositional environments (Moldowan et al. 1985; Subroto et al. 1991).

Table 3. Key GC-MS data from source rocks in the Gulf of Suez Rift basin

No.	Well	Depth (m)	Fm	R1	R2	R3	R4	R5	R6	R7	R8	R9	R10	R11	R12	R13	R14	R15	R16	R17	R18
1	Geisum	1210	Belayim	0.11	0.20	0.57	0.67	0.06	0.48	1.73	0.75	1.56	0.51	32.5	32.1	35.4	0.09	0.08	0.24	5.65	3.02
2	Amal	1862	Belayim	0.05	0.46	0.5	0.45	0.07	0.44	1.88	0.86	2.02	0.54	52.9	20.6	26.4	0.09	0.09	0.06	3.72	3.37
3	Morgan	2408	Rudeis	0.04	0.19	0.79	0.42	0.08	0.48	2.0	0.73	1.0	0.59	39.5	32.6	27.9	0.32	0.51	0.69	0.93	0.93
4	North Shadwan-1	3347	Rudeis	0.08	0.05	0.38	0.89	0.06	0.51	3.18	0.52	0.67	0.52	35.9	32.7	31.4	0.30	0.19	0.63	3.57	0.53
5	Ras Ghara-1	3400	Rudeis	0.07	0.66	0.42	0.66	0.06	0.52	1.88	0.57	0.89	0.58	34.0	34.0	32.0	0.52	0.51	0.72	0.56	0.56
6	Ras Ghara-2	3415	Rudeis	0.04	1.01	0.31	0.31	0.05	0.52	2.10	0.6	0.88	0.57	42.0	31.0	27.0	0.54	0.64	0.47	0.48	0.66
7	Ras Ghara-3	3465	Rudeis	0.09	0.64	0.59	0.60	0.08	0.54	2.25	0.64	0.94	0.59	37.0	32.0	31.0	0.44	0.54	0.57	0.66	0.66
8	Ras Ghara-3	3520	Rudeis	0.07	0.14	0.69	0.60	0.05	0.52	2.21	0.59	0.84	0.61	37.0	33.0	30.0	0.48	0.54	0.62	0.81	0.81
9	Belayim Land	4050	Rudeis	0.03	0.21	0.79	0.36	0.09	0.56	2.38	0.9	0.92	0.59	42.8	30.8	26.4	0.35	0.52	0.76	0.83	0.83
10	Ras Ghara-4	2010	Nukhul	0	0.25	0.70	0.45	0.03	0.58	2.35	0.55	1.31	0.57	35.0	32.9	32.1	0.37	0.46	0.43	3.41	0.61
11	Ras Ghara-4	2016	Nukhul	0	0.25	0.77	0.45	0.04	0.57	2.50	0.56	1.43	0.57	34.5	33.6	31.9	0.39	0.46	0.5	2.74	0.63
12	Ras Ghara-4	2169	Nukhul	0	0.23	0.77	0.45	0.03	0.57	2.33	0.57	1.34	0.52	36.5	32.4	31.1	0.38	0.47	0.54	2.63	0.61
13	Geisum	2316	Nukhul	0.05	0.6	0.33	0.47	0.09	0.55	1.77	0.59	1.16	0.46	42.5	23.1	34.4	0.20	0.12	0.46	2.15	0.40
14	Ras Ghara-3	3615	Nukhul	0.07	0.81	0.81	0.55	0.08	0.58	1.26	0.62	0.79	0.56	37.0	35.0	28.0	0.46	0.58	0.6	0.54	0.54
15	Amer	948	Thebes	0.03	0.14	0.78	0.32	0.03	0.49	1.92	0.69	1.27	0.59	32.5	33.0	34.6	0.41	0.42	0.33	3.5	0.47
16	Amal	2716	Thebes	0	0.09	0.68	0.56	0.07	0.60	1.75	0.81	1.31	0.58	37.1	28.2	34.7	0.41	0.44	0.39	2.26	0.34
17	Sinai	3090	Thebes	0.03	0.68	0.42	0.42	0.09	0.50	1.79	0.71	0.81	0.59	38.0	33.0	28.0	0.52	0.61	0.49	0.74	0.74
18	Morgan	3094	Thebes	0.05	0.17	0.77	0.42	0.09	0.47	2.04	0.76	1.01	0.59	39.6	31.9	28.5	0.29	0.47	0.69	0.89	0.89
19	October-A	3139	Thebes	0.05	0.15	0.71	0.39	0.03	0.69	1.93	0.64	0.88	0.59	29.1	31.9	39.0	0.45	0.47	0.50	3.45	0.41
20	Belayim Marine	3210	Thebes	0.02	0.15	0.92	0.25	0.03	0.7	2.93	0.72	1.36	0.59	34.3	31.3	34.4	0.43	0.52	0.22	3.76	0.29
21	Belayim Marine	3216	Thebes	0.03	0.14	0.91	0.45	0.03	0.71	2.96	0.73	1.35	0.60	34.6	31.4	34.0	0.40	0.54	0.33	3.6	0.30
22	July	3502	Thebes	0.03	0.10	0.93	0.37	0.07	0.5	2.17	0.63	0.98	0.59	40.4	32.0	27.6	0.37	0.61	0.68	1.06	1.06
23	SB 276	3871	Thebes	0.1	0.23	0.72	0.82	0.05	0.59	1.74	0.70	1.36	0.58	32.4	30.6	37.0	0.46	0.43	0.56	3.76	0.51
24	Geisum	2560	Esna	0.04	0.27	0.65	0.52	0.06	0.42	1.80	0.52	1.31	0.59	36.0	32.2	31.8	0.43	0.41	0.65	3.56	0.73
25	Sinai	3100	Esna	0	0.30	0.63	0.28	0.03	0.39	2.35	0.76	1.12	0.58	32.0	33.0	35.0	0.33	0.29	0.75	0.63	0.63
26	Amer	1149	Br. LS	0.03	0.19	0.78	0.47	0.09	0.52	1.69	0.51	1.30	0.56	37.7	29.6	32.8	0.28	0.27	0.39	3.24	0.77
27	Ras Ghara-4	2208	Br. LS	0	0.23	0.68	0.30	0.03	0.60	2.40	0.63	1.31	0.56	34.4	33.0	32.6	0.34	0.42	0.43	2.53	0.71
28	Geisum	2682	Br. LS	0.05	0.15	0.75	0.54	0.06	0.59	1.88	0.59	1.31	0.59	37.0	32.1	30.9	0.46	0.44	0.62	3.31	0.65
29	Amal	2807	Br. LS	0.02	0.13	0.59	0.54	0.10	0.57	1.60	0.64	0.98	0.57	36.6	33.4	30.0	0.47	0.46	1.42	3.87	0.65
30	Sinai	3120	Br. LS	0	0.29	0.50	0.49	0.10	0.55	2.20	0.69	1.06	0.61	33.0	33.0	34.0	0.52	0.62	0.58	0.82	0.82
31	October-A	3554	Br. LS	0	0.12	0.82	0.35	0.04	0.57	1.72	0.74	1.29	0.58	32.0	33.2	34.8	0.45	0.46	0.27	4.06	1.40
32	July	3566	Br. LS	0.03	0.09	0.88	0.37	0.08	0.51	2.0	0.61	0.95	0.61	40.0	32.3	27.7	0.37	0.62	0.71	1.02	1.02
33	October-B	3590	Br. LS	0.01	0.11	0.62	0.3	0.12	0.43	2.0	0.66	1.30	0.60	36.6	32.9	30.4	0.39	0.60	0.43	0.47	0.47
34	North Shadwan-2	3669	Br. LS	0.04	0.37	0.75	0.75	0.01	0.60	2.45	0.36	1.43	0.57	33.6	33.1	33.3	0.53	0.54	0.29	3.39	0.45
35	SB 276	4081	Br. LS	0.11	0.22	0.51	1.17	0.10	0.61	1.08	0.45	1.25	0.58	30.9	34.2	34.9	0.49	0.45	0.76	3.81	0.87
36	Belayim Land	4722	Br. LS	0.03	0.22	0.84	0.36	0.07	0.61	1.96	0.72	0.85	0.59	43.2	30.9	25.9	0.34	0.51	0.78	0.84	0.84
37	Sinai	3180	Matulla	0.04	1.02	1.02	1.02	0.15	0.08	1.93	0.65	0.93	0.59	34.0	33.0	33.0	0.43	0.49	0.57	0.55	0.55
38	North Shadwan-2	3749	Matulla	0.05	0.20	0.99	0.25	0.14	0.49	1.73	0.71	1.08	0.55	36.6	29.9	33.5	0.39	0.44	0.78	4.26	0.35
39	SB 276	4124	Matulla	0.13	0.21	0.52	1.08	0.10	0.49	1.21	0.53	1.30	0.58	29.5	34.3	36.2	0.50	0.47	0.81	3.71	0.77

R1, oleane/hopane; R2, gammacerane/hopane; R3, norhopane/hopane; R4, Ts/Tm; R5, C₁₉/C₂₃ tricyclic terpanes; R6, C₂₂/C₂₁ tricyclic terpanes; R7, C₂₃/C₂₄ tricyclic terpanes; R8, C₂₄ tetracyclic terpanes/C₂₆ tricyclic terpanes; R9, C₃₅/C₃₄ extended hopanes; R10, C₃₂ 22S/(22S + 22R) homohopanes; R11, %C₂₇ *axaxR*; R12, %C₂₈ *axaxR*; R13, %C₂₉ *axaxR*; R14, C₂₉ 20S/(20S + 20R); R15, C₂₉ $\beta\beta$ ($\beta\beta$ + *ax*); R16, C₂₇ diasteranes/regular steranes; R17, %C₃₀ *axaxR*; R18, Steranes/hopanes

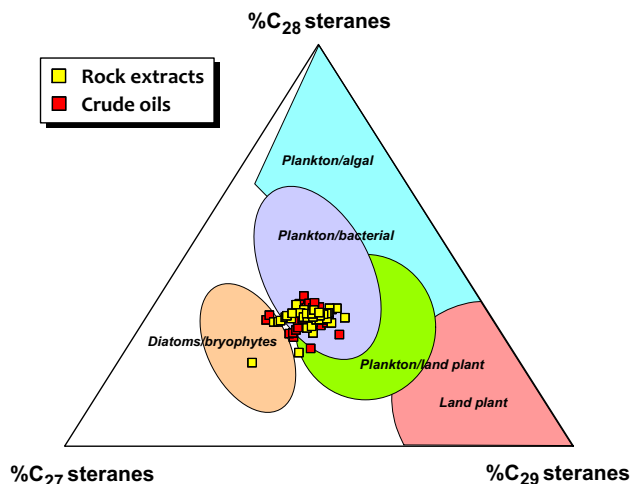


Fig. 10. C_{27} – C_{28} – C_{29} sterane ($\alpha\alpha\alpha$ 20R isomers) ternary diagram shows that most of the extracts plot in a close cluster within the area ascribed to plankton/bacterial organic matter (see Hunt 1996).

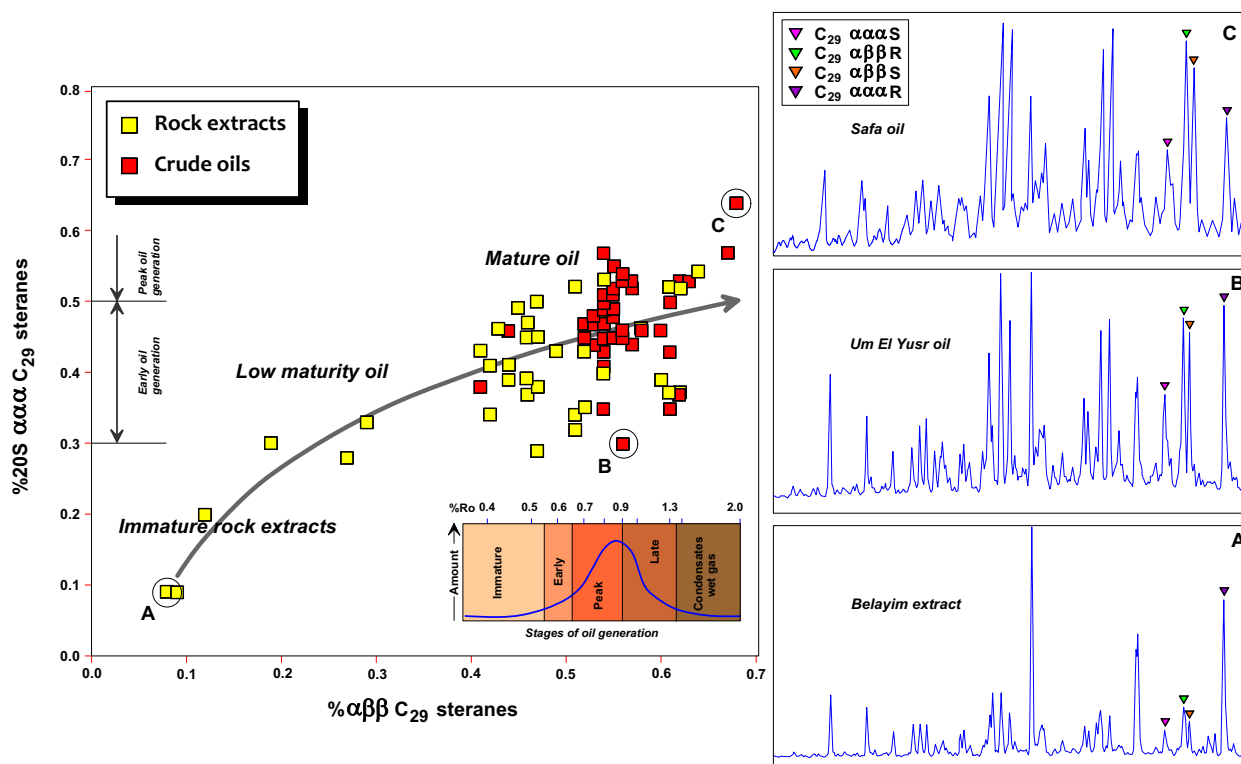


Fig. 11. Relative thermal maturity for the Gulf of Suez crude oils and sediments based on two C_{29} sterane stereoisomer ratios. Inset shows the approximate amount of hydrocarbons yield relative to the oil generation window and vitrinite reflectance, $\%R_o$ (see Peters et al. 2005).

Important characteristics of the m/z 191 mass fragmentograms (Fig. 8) for the extracted bitumens are abundant gammacerane (up to 0.37 in the Brown Limestone sample no. 34) and the absence or the

presence of very little, if any, oleanane. Gammacerane/hopane and oleanane/hopane (Table 3) are sensitive to carbonates and angiosperms (flowering-plant input), respectively. This implies that the

Table 4. Geologic, stable carbon isotopic, elemental composition, and gas chromatographic data for crude oils from the Gulf of Suez Rift basin

No.	Field	Well name	Reservoir	Depth (m)	$\delta^{13}C$ Sat ^a	$\delta^{13}C$ Aro ^a	CV	API (°)	% S (wt%)	Ni (ppm)	V (ppm)	V/Ni	Ph/n-C ₁₈	Pr/n-C ₁₇	Pr/Ph
1	Morgan	Morgan-1			-29.3	-28.4	-0.57	20.0	4.31	203	329	1.62	0.40	0.33	0.88
2	Morgan	Morgan-2			-29.0	-28.1	-0.66	24.0	1.66	10	40	4.0	0.34	0.31	0.94
3	October	October	Kareem		-28.3	-27.6	-1.32	27.0	2.11	77	35	0.45	0.41	0.35	0.92
4	July	July A			-28.6	-27.6	-0.56	30.8	1.44	19.6	24.1	1.23	0.51	0.37	0.77
5	July	July B			-28.7	-27.9	-0.98	26.2	1.69	41.1	49.7	1.21	0.53	0.37	0.76
6	July	July C			-28.3	-27.6	-1.32	29.7	1.10	13.6	16.4	1.20	0.49	0.36	0.77
7	Ramadan	Ramadan-1			-28.8	-27.6	-0.06	29.3	1.09	12.6	18.4	1.46	0.54	0.42	0.84
8	Ramadan	Ramadan-2			-28.7	-27.5	-0.09	29.7	1.29	8.4	12.1	1.44	0.53	0.44	0.85
9	South Gharib	South Gharib-1			-28.5	-27.8	-1.26	28.4	1.57	22.8	27.2	1.19	0.49	0.35	0.75
10	South Gharib	South Gharib-2			-28.6	-27.7	-0.79	30.5	1.52	23.9	27.5	1.15	0.51	0.38	0.77
11	Sidri	Sidri	Matulla	3492-3606	-29.2	-28.7	-1.49	16.8	2.54	41.5	96.4	2.32	0.93	0.62	0.68
12	Abu Rudeis	Abu Rudeis-1	Nukhul	2519-2647				22.6	2.52				0.79	0.56	0.73
13	Abu Rudeis	Abu Rudeis-2	Nubia	3391-3395				19.9	3.69				1.03	0.68	0.69
14	Abu Zenima	Abu Zenima	Matulla	3753-3770				19.1	3.66				0.89	0.59	0.73
15	Abu Rudeis	Abu Rudeis-3	Matulla	3177-3198				21.1	3.49				0.93	0.6	0.71
16	Abu Rudeis	Abu Rudeis-4	Matulla					12.8	1.44				0.87	0.54	0.66
17	Abu Rudeis	Abu Rudeis-5	Thebes					14.3	1.05				0.76	0.49	0.70
18	Zaafarana	Zaafarana	Rudeis		-28.27	-27.29	-0.71		3.60				0.55	0.32	0.59
19	Bakr	Bakr	Nukhul		-29.41	-28.56	-0.64		3.90				0.71	0.46	0.67
20	Um El Yusr	Um El Yusr	Rudeis		-28.98	-28.26	-1.07		1.97				0.43	0.38	0.95
21	Ras Ghara	Ras Ghara-1	Nukhul	1995-1998	-29.0	-28.6	-1.77						0.54	0.41	0.56
22	Ras Ghara	Ras Ghara-2	Kareem	2384-2440	-29.5	-28.6	-0.51						0.49	0.4	0.85
23	Ras Ghara	Ras Ghara-3	Rudeis	2384-2440	-29.4	-28.5	-0.54						0.52	0.39	0.87
24	Ras Ghara	Ras Ghara-4	Matulla	2962-2980	-30.1	-29.4	-0.76						0.39	0.36	0.54
25	Ras Ghara	Ras Ghara-5	Kareem	3044-3084	-24.5	-22.6	-0.16						0.55	0.47	1.37
26	Ras Ghara	Ras Ghara-6	Matulla	3665-3700	-29.8	-29.1	-0.86						0.58	0.53	0.65
27	Sinai	Sinai A	Kareem	2142-2154	-28.1	-27.6	-1.83						0.51	0.49	0.97
28	Sinai	Sinai B	Rudeis	2017-2040	-27.9	-27.7	-2.56						0.52	0.44	1.0
29	Sinai	Sinai C	Rudeis	2090-2130	-27.7	-27.9	-3.51						0.52	0.45	1.0
30	Sinai	Sinai D	Kareem	2338-2350	-28.3	-28.6	-3.54						0.48	0.43	0.81
31	Belayim Marine	Belayim Marine	Rudeis					15.9					0.65	0.43	0.71
32	Abu Rudeis	Abu Rudeis-6			-29.4	-28.6	-0.76						0.48	0.31	0.71
33	Abu Rudeis	Abu Rudeis-7			-29.6	-28.5	-0.03	21.6					0.46	0.36	0.76
34	Abu Rudeis	Abu Rudeis-8	Nubia	4120-4222	-29.8	-29.0	-0.64	12.0	1.69		72.0		0.57	0.36	0.63
35	Abu Rudeis	Abu Rudeis-9			-29.3	-28.2	-0.12						0.56	0.35	0.62
36	North Shadwan	North Shadwan-1	Matulla	3690	-30.2	-29.1	-0.15	25.5	1.99	1.0	1.0	1.0	0.41	0.26	0.48
37	North Shadwan	North Shadwan-2			-29.3	-28.2	-0.12		0.87	82.3	1.0	0.01	0.57	0.39	0.76
38	North Shadwan	North Shadwan-3			-29.3	-28.2	-0.12	35.2	0.89	2.6	6.5	2.50	0.59	0.39	0.74
39	North Shadwan	North Shadwan-4			-29.3	-28.3	-0.35	36.4	0.91	2.6	1.0	0.38	0.32	0.39	1.36
40	North Shadwan	North Shadwan-5			-29.3	-28.3	-0.35	35.4	0.94	4.5	7.8	1.73	0.58	0.4	0.75
41	Safa	Safa			-29.1	-27.9	0.03	23.0	1.29	21.0	1.0	0.04	0.32	0.27	0.89
42	Warda	Warda			-29.0	-27.7	0.23	35.0	0.53	7.0	1.0	0.14	0.32	0.26	0.88

Table 4. continued

No.	Field	Well name	Reservoir	Depth (m)	$\delta^{13}\text{C}_{\text{Sat}}^{\text{a}}$	$\delta^{13}\text{C}_{\text{Aro}}^{\text{a}}$	CV	API ($^{\circ}$)	% S (wt%)	Ni (ppm)	V (ppm)	V/Ni	Ph/n-C ₁₈	Pr/n-C ₁₇	Pr/Ph
43	Edfu	Edfu		3356	-28.5	-27.5	-0.59		0.71	6.5	18.6	2.86			
44	Saqqara	Saqqara-1		4221	-28.1	-26.8	-0.05	41.3	0.34	1.1	1.0	0.90	0.37	0.37	1.08
45	Saqqara	Saqqara-2		4402	-28.2	-26.9	-0.02	38.4	0.47	1.0	1.0	1.0	0.42	0.37	0.91
46	Saqqara	Saqqara-3		4527	-27.9	-26.8	-0.56	39.3	0.62				0.38	0.41	1.28

$\delta^{13}\text{C}_{\text{Sat}}$ and $\delta^{13}\text{C}_{\text{Aro}}$, stable carbon isotope ratios (relative to PDB standard, ‰) for saturated and aromatic hydrocarbon fractions; CV, canonical variable = $-2.53\delta^{13}\text{C}_{\text{Sat}} + 2.22\delta^{13}\text{C}_{\text{Aro}} - 11.65$; API, American Petroleum Institute gravity; S, sulfur wt%; Ni, nickel in ppm; V, vanadium in ppm; Ph/n-C₁₈, phytane/n-octadecane ratio; Pr/n-C₁₇, pristane/n-heptadecane ratio; Pr, pristane; Ph, phytane; Pr/Ph, pristane/phytane ratio

analyzed samples were deposited in stratified anoxic water (saline to hypersaline) with significant halophilic bacterial input (Moldowan et al. 1985; Brassell et al. 1988; Zumberge 1987; Moldowan et al. 1994; Sinninghe Damsté et al. 1995; Peters et al. 2005). The pervasive anoxic depositional environment for these sediments is likewise confirmed by C₃₅/C₃₄ extended homohopanes > 1 (Peters and Moldowan 1991; Dahl et al. 1994; Sinninghe Damsté et al. 1995). Simultaneously, the low abundance of Ts relative to Tm, except two samples from the Brown Limestone (sample no. 35) and the Matulla Formation (sample no. 39) where the ratio of Ts/Tm > 1.0 (Table 3), indicates low-maturity or low-clay shale/marl or carbonate source rocks.

The sterane ternary plot (Fig. 10) shows that the majority of the extract samples plot in a close cluster within the area characterized by plankton/bacterial organic matter (Hunt 1996) with the C₂₇ steranes more abundant (up to 53%) than the C₂₉ homologues and relatively high C₂₈ steranes (up to 35%). The predominance (sometimes present in equal amounts) of C₂₇ over C₂₉ steranes together with high C₃₀ 24-n-propylcholestanes suggests the presence of marine algal organic matter with minor terrigenous input deposited in anoxic to a mildly reducing environment (Moldowan et al. 1985; Peters et al. 1999). The relative amount of diasteranes and regular steranes is variable (Table 3), but is thought to be primarily due to maturity effects in which the more mature samples show higher concentrations of the more stable rearranged steranes (Rubinstein et al. 1975).

Thermal Maturity of the Gulf of Suez Sediments

Thermal maturity consists of temperature/time-driven disproportionation reactions that convert sedimentary organic matter into light and heavy fractions of petroleum and finally into hydrocarbon gas and pyrobitumen or graphite (Peters et al. 2005). During diagenesis and catagenesis terpanes and steranes undergo a series of conversions via reduction, rearrangement, and isomerization, resulting in new compounds (Mostafa 1993; Hunt 1996). Different geochemical scales commonly used to describe the extent of thermal maturation include Rock-Eval T_{max} and biomarker maturity ratios (cf. Peters et al. 2005).

Pyrolysis T_{max} values vary considerably in the analyzed samples from immature (414 °C in the

Rudeis Formation) to peak oil window with $T_{\max} \sim 447$ °C (Table 1; Fig. 6).

The most commonly used biomarker ratios to assess thermal maturity are based on isomerization of hydrogen atoms around asymmetric carbon atoms at C-20 [$\%20S/(20S + 20R)$] and C-14 and C-17% $\beta\beta/(\beta\beta + \alpha\alpha)$ in the steranes, and C-22 in the hopanes [$\%22S/(22S + 22R)$] (Mackenzie and McKenzie 1983; Seifert and Moldowan 1986; Peters et al. 2005).

The ratio of diasteranes to regular steranes is variable, but is thought to be primarily due to maturity effects with the more mature samples showing a higher diasteranes.

The plot of $\%20S/(20S + 20R)$ and $\% \beta\beta/(\beta\beta + \alpha\alpha)$ C₂₉ steranes (Fig. 11) shows that the majority of the Gulf of Suez source rocks were not buried deeper than the early oil generation window and generally the extract samples vary from immature to the main stage of oil window with $\%R_o$ ranging from < 0.6 to < 0.9 . The same conclusion is also supported by the C₃₂ 22S/(22S + 22R) homohopane ratios (Table 3).

Oil Geochemistry

Elemental, Bulk, and Isotopic Composition

Forty-six crude oil samples (Table 4) were analyzed to define the bulk and molecular geochemical characteristics, identify oil families, and establish genetic relationships with the inferred source rock facies in the Gulf of Suez basin. The studied oils were retrieved from 19 oilfields from both sandstone and carbonate pay-zones ranging in age from Cretaceous to Miocene (145.0–23.0 Ma).

The Gulf of Suez oils exhibit a wide range of API gravity from heavy oils (API $\sim 12^\circ$) to medium-light oils (API $\approx 41^\circ$). Most of the analyzed oils are of the heavy–medium range, where Abu Rudeis-8 has the lowest API gravity and Saqqara-1 has the highest API value (Table 4). In accordance with this wide range in API gravities, sulfur content of the oils ranges from 0.34 wt% (Saqqara-1 oil) to 4.31 wt% (Morgan-1 oil) with an average 1.78 wt%. As observed in Figure 12, there is an inverse relation between API gravity and sulfur content in the Gulf of Suez oils where the quantity of sulfur decreases with increasing oil gravity and increasing thermal maturity. The overall low API gravity and high sulfur content are consistent with anoxic depositional

environments often associated with carbonate-facies source rocks (Clark and Philp 1989; Subroto et al. 1991). Interestingly, the systematic increase of API gravity from north to south (Fig. 12) is consistent with more extensive crustal extension and thermal subsidence of the southern sector than the central and northern provinces of the Suez Rift (Steckler et al. 1988). The average geothermal gradient in the southern sector of the Gulf of Suez is $- 16.81$ °C/30.48 m, whereas it is $- 16.91$ °C/30.48 m in the northern and central sectors (Steckler 1985; Alsharhan and Salah 1994, 1997; Alsharhan 2003). Accordingly, most variations in API gravity are believed to be related to the maturity at which the oil was generated (Alsharhan and Salah 1997; Wever 1999, 2000; Alsharhan 2003).

Vanadium (V) and nickel (Ni) are important trace elements in crude oils. The Gulf of Suez oils contain more vanadium than nickel (Table 4). The general increasing of V and Ni contents with decreasing gravity is a reflection of the increase in heavy ends containing the metal–porphyrin complexes in the oils with low API gravity (Lewan 1984; Moldowan et al. 1986; Hunt 1996). The analyzed oils have wide-ranging V/Ni ratios from 0.01 to 2.86 (Table 4), implying more than a single source for the oils or similar source rocks with different maturity histories (El Diasty and Peters 2014; El Diasty et al. 2015a).

With increasing thermal maturity, kerogen becomes isotopically heavier (more positive) and a more ^{13}C -rich mature oil will be generated (Rohrbach 1983). The stable carbon isotope results for the oil samples show a wide range of values of $- 30.2$ to $- 24.5\%$ for the saturated hydrocarbons and $- 29.4$ to $- 22.6\%$ for the aromatic hydrocarbon fractions. The relationship between the aromatic ($\delta^{13}\text{C}_{\text{aro}}$) and saturated ($\delta^{13}\text{C}_{\text{sat}}$) fraction carbon isotopes for the Gulf of Suez oils suggests their origin from source rock containing predominantly marine-derived organic matter, deposited in a restricted marine environment where the contribution of land-derived organic matter was limited (Fig. 7). This finding is supported by the canonical variable values of less than 0.47 (Sofer 1984). An outlier sample from Ras Ghara-5 oil deviates from the expected cluster of the Gulf of Suez oil (Fig. 7). Differences in source bed depositional environment, thermal maturity, and migration history can affect the crude oil bulk and isotopic compositions. The heavy stable carbon isotopic composition of the Ras Ghara-5 oil is like terrigenous oils from the north Western Desert. The

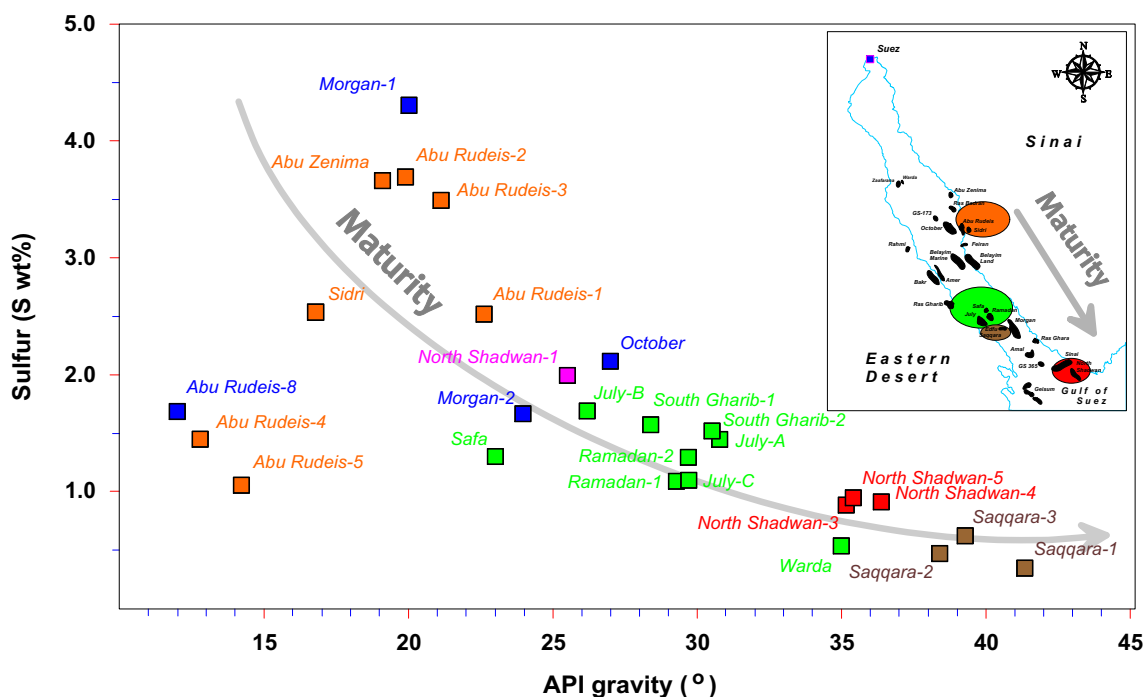


Fig. 12. Relationship between API gravity ($^{\circ}$) and sulfur content (wt%) for the Gulf of Suez oils.

unusual ^{13}C -rich signature of this oil sample may result from mixed terrigenous and marine source organic input and/or higher thermal maturity. Nile Delta condensates (El Diasty et al. 2019b) and the Western Desert oil samples (Zein El Din et al. 1990) exhibit a less negative isotopic signature, typical for terrigenous or waxy oils. Isotopic changes caused by maturity differences in a suite of oils probably do not exceed 2.0‰. Different source rocks can result in isotopic variations in generated oil of larger magnitude, which could easily obscure the effects of maturity (Sofer 1984).

Normal Alkanes and Acyclic Isoprenoids

On the basis of GC chromatograms (Fig. 13), nearly all Gulf of Suez oils have *n*-alkane distributions biased toward low molecular weight $< n\text{-C}_{20}$. The predominance of light compounds suggests that these oils were derived from lipids synthesized by phytoplankton/benthic algae and bacterial organic matter with less contribution of terrigenous organic debris (Philp 1985; Peters et al. 2005). In our study and other pioneer works on the Gulf of Suez oils (Rohrback 1983; Mostafa 1993; Alsharhan and Salah

1997; Wever 2000; Alsharhan 2003; El Diasty and Peters 2014; El Diasty et al. 2015a, b), no apparent evidence of biodegradation was recognized. Some of the analyzed oils (e.g., Sidri oil), show an elevated GC baseline, which often represents a complex mixture of cyclic compounds, and also is common in oils from carbonate source rocks (Palacas et al. 1984; Grice et al. 1998; Peters et al. 2005; El Diasty et al. 2015a).

For most oils the Pr/Ph ratios is less than unity, which suggests derivation from marine organic matter deposited under highly reducing to anoxic environments. Some samples from the Shadwan, Ras Ghara, Sinai, and Saqqara oilfields in the southern Suez Rift have Pr/Ph ratios slightly > 1 , together with a systematic increase in API gravity (Table 4). This variation in isoprenoids ratios can be attributed to changes in redox conditions of separate source facies (Mostafa 1993; El Diasty et al. 2015a). The Gulf of Suez oils show Pr/*n*-C₁₇ and Ph/*n*-C₁₈ ratios consistent with an origin from anoxic carbonate/marl source rocks (marine algal Type II kerogens; Fig. 9) deposited under anoxic conditions (Peters et al. 1999) that underwent different thermal histories.

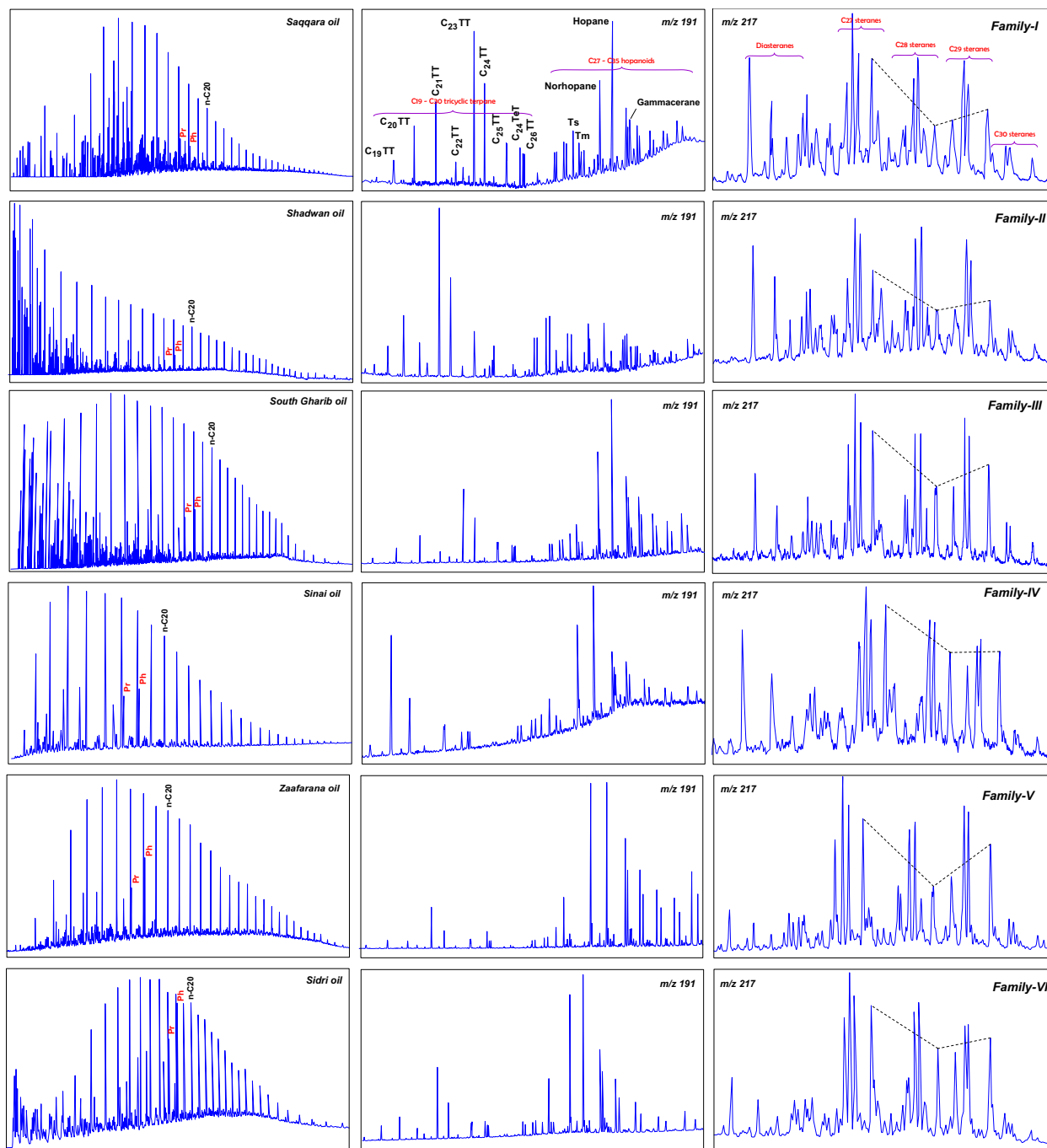


Fig. 13. GC-SIM for terpane (m/z 191) and sterane (m/z 217) mass fragmentograms of saturated hydrocarbon fractions for selected oil samples from the Gulf of Suez.

Terpanes and Steranes

Table 5 summarizes some of the representative terpane and sterane biomarkers that have been used

in the current work for determining organic matter precursors, depositional paleoenvironment, biodegradation, thermal maturation, and age of the putative source rocks for the oils (Hunt 1996; Peters

Table 5. Key GC–MS data from oils in the Gulf of Suez Rift basin

No.	R1 ^a	R2 ^a	R3 ^a	R4 ^a	R5 ^a	R6 ^a	R7 ^a	R8 ^a	R9 ^a	R10 ^a	R11	R12 ^a	R13 ^a	R14 ^a	R15 ^a	R16
1	0.05	0.78	0.43	0.69	0.89	0.52	0	0.74	0.01	0.19	0.57	1.46	34.0	31.9	34.1	0.35
2	0.07	0.49	0.66	0.75	0.65	0.59	0	0.66	0.01	0.21	0.58	1.34	34.5	29.5	36.0	0.41
3	0.06	0.52	0.51	0.86	0.69	0.44	0	0.80	0.10	0.08	0.57	1.20	35.4	32.9	31.7	0.48
4	0.08	0.42	0.61	0.79	0.64	0.75	0.04	0.75	0.07	0.24	0.58	1.31	32.9	33.5	33.5	0.48
5	0.06	0.41	0.61	0.77	0.63	0.61	0.04	0.74	0.05	0.23	0.58	1.30	33.6	31.8	34.5	0.47
6	0.09	0.41	0.62	0.84	0.63	0.92	0.04	0.63	0.08	0.35	0.58	1.31	30.5	33.6	36.0	0.47
7	0.08	0.29	0.80	0.79	0.57	0.69	0.04	0.75	0.08	0.21	0.58	1.50	34.8	32.4	32.8	0.49
8	0.10	0.32	0.79	0.79	0.59	0.75	0.04	0.66	0.07	0.37	0.58	1.38	32.12	33.1	34.6	0.50
9	0.08	0.43	0.61	0.79	0.62	0.71	0.04	0.74	0.06	0.22	0.59	1.31	32.4	32.8	34.8	0.47
10	0.09	0.41	0.60	0.80	0.63	0.78	0.05	0.74	0.06	0.23	0.58	1.31	34.3	30.8	34.9	0.47
11	0.05	0.47	0.71	0.82	0.69	0.23	0.01	0.78	0.03	0.11	0.60	1.41	35.3	30.4	34.3	0.49
12	0.06	0.48	1.01	0.80	0.68	0.29	0.02	0.89	0.05	0.09	0.61	0.99	34.0	32.0	34.0	0.53
13	0.04	0.52	0.89	0.78	0.58	0.23	0.01	0.75	0.03	0.11	0.60	1.12	33.6	32.8	33.6	0.51
14	0.05	0.51	0.92	0.71	0.69	0.23	0.01	0.88	0.03	0.11	0.58	1.09	44.5	31.1	24.5	0.55
15	0.04	0.51	0.92	0.79	0.59	0.23	0.01	0.81	0.04	0.12	0.60	1.09	33.5	32.1	34.4	0.51
16	0.05	0.52	0.94	0.80	0.68	0.24	0.01	0.87	0.03	0.11	0.60	1.06	34.2	32.2	33.6	0.52
17	0.05	0.49	0.92	0.73	0.66	0.25	0.01	0.83	0.04	0.12	0.58	1.09	43.2	32.1	24.7	0.57
18	0.02	0.86	0.41	0.82	1.16	0.41	0.01	0.99	0.04	0.10	0.59	1.54	34.9	30.8	34.3	0.37
19	0.02	0.67	0.5	0.82	0.67	0.31	0.01	0.77	0.03	0.11	0.60	1.29	31.3	32.0	33.7	0.35
20	0.04	0.47	0.58	0.82	0.67	0.57	0.04	0.62	0.05	0.14	0.60	1.23	33.5	33.8	32.7	0.30
21	0.09	0.59	0.81	0.77	0.42	0.40	0	0.78	0.04	0.28	0.55	1.30	34.0	34.0	32.0	0.45
22	0.08	0.62	0.68	0.77	0.61	0.73	0	0.74	0.05	0.34	0.56	1.28	35.0	34.0	31.0	0.53
23	0.09	0.55	0.67	0.75	0.48	0.81	0	0.7	0.04	0.29	0.54	1.11	33.0	35.0	32.0	0.53
24	0.08	0.56	0.66	0.78	0.82	0.38	0	0.76	0.02	0.31	0.57	1.17	34.0	35.0	31.0	0.50
25	0.09	0.44	0.65	0.73	0.77	1.71	0	0.39	0.24	0.06	0.55	0.97	34.0	37.0	29.0	0.38
26	0.07	0.69	0.67	0.77	0.69	0.81	0	0.66	0.04	0.52	0.57	1.01	36.0	35.0	29.0	0.57
27	0.08	0.44	0.65	0.75	0.72	0.86	0	0.59	0.10	0.23	0.55	1.19	33.0	34.0	33.0	0.46
28	0.07	0.38	0.66	0.78	0.58	0.74	0	0.59	0.11	0.20	0.56	1.08	32.0	35.0	32.0	0.43
29	0.08	0.40	0.68	0.72	0.67	0.86	0	0.54	0.13	0.21	0.57	1.10	33.0	34.0	33.0	0.45
30	0.09	0.45	0.64	0.70	0.54	0.58	0	0.77	0.07	0.28	0.59	1.02	36.0	33.0	31.0	0.46
31	0.06	0.52	0.37	0.77	0.73	0.41	0.01	0.86	0.04	0.13	0.60	1.21	34.6	31.8	33.6	0.43
32	0.04	0.54	0.59	0.76	0.61	0.25	0.03	0.65	0.03	0.19	0.59	1.24	32.5	30.7	36.8	0.45
33	0.04	0.49	0.54	0.73	0.51	0.25	0.02	0.78	0.04	0.22	0.61	1.26	32.8	30.4	36.8	0.46
34	0.03	0.5	0.52	0.75	0.63	0.25	0.02	0.75	0.01	0.15	0.57	1.30	33.3	33.5	33.2	0.48
35	0.03	0.48	0.58	0.72	0.59	0.27	0.03	0.75	0.02	0.20	0.60	1.14	33.1	33.7	33.2	0.47
36	0.03	0.49	0.67	0.63	0.22	0.61	0.04	0.58	0.02	0.75	0.59	1.63	33.7	34.3	32.0	0.44
37	0.06	0.55	0.59	0.72	0.23	1.70	0.10	0.89	0.01	0.60	0.60	1.39	39.2	29.1	31.7	0.41
38	0.05	0.72	0.58	0.71	0.21	1.94	0.10	0.94	0	0.77	0.61	1.80	40.8	27.7	31.5	0.46
39	0.05	0.66	0.57	0.71	0.22	2.03	0.10	0.96	0.01	0.80	0.60	1.40	41.5	27.4	31.1	0.44
40	0.05	0.70	0.59	0.69	0.21	1.86	0.11	0.97	0.01	0.76	0.60	1.40	41.3	26.6	32.1	0.45
41	0.09	0.44	0.79	0.76	0.63	0.73	0.02	0.73	0.02	0.32	0.58	1.50	39.5	23.8	36.8	0.64
42	0.11	0.47	0.79	0.75	0.60	0.71	0.03	0.72	0.03	0.29	0.58	1.38	32.1	27.2	40.7	0.43
43	0.11	0.33	0.81	0.79	0.53	1.29	0.08	0.63	0.03	0.35	0.56	1.28	35.3	32.0	32.7	0.52
44	0.14	0.27	0.82	0.88	0.46	2.09	0.20	0.60	0.13	0.46	0.56	1.04	38.3	30.9	30.8	0.54
45	0.14	0.30	0.77	0.87	0.58	2.47	0.13	0.63	0.15	0.42	0.56	1.25	37.3	31.2	31.5	0.53
46	0.17	0.35	0.64	0.81	0.56	1.25	0.12	0.68	0.13	0.39	0.58	1.20	39.7	28.5	31.8	0.49
No.	R17	R18 ^a	R19 ^a	R20 ^a	R21	R22	R23	R24	R25	R26	R27	R28				
1	0.54	0.56	3.87	0.44	0.18	0.77	0.67	1.39	1.5	0.22	27.12	1.2				
2	0.54	0.42	3.77	0.35	0.21	0.77	0.67	1.0	0.93	0.46	21.14	1.07				
3	0.55	0.48	3.92	0.45	0.26	0.78	0.69	0.99	1.14	0.45	26.64	0.85				
4	0.53	0.51	3.47	0.71	0.44	0.82	0.74	1.01	0.99	0.37	23.07	1.2				
5	0.53	0.49	2.93	0.63	0.36	0.81	0.73	1.03	0.98	0.49	24.05	1.1				
6	0.54	0.47	3.41	0.76	0.55	0.84	0.79	0.99	0.9	0.61	24.28	1.14				
7	0.55	0.6	2.92	0.83	0.44	0.80	0.72	1.11	0.78	0.56	21.19	0.96				
8	0.54	0.5	3.28	0.89	0.52	0.81	0.73	1.11	0.9	0.42	21.88	1.02				
9	0.53	0.51	3.21	0.67	0.41	0.81	0.74	0.99	0.99	0.53	25.22	1.14				
10	0.52	0.55	3.36	0.64	0.43	0.81	0.73	1.03	1.02	0.34	22.74	1.21				

Table 5. continued

No.	R17	R18 ^a	R19 ^a	R20 ^a	R21	R22	R23	R24	R25	R26	R27	R28
11	0.54	0.22	2.52	0.38	0.34				1.99	0.33	32.39	1.23
12	0.56	0.24	2.05	0.67	0.50				1.39	0.45	27.39	0.93
13	0.54	0.2	2.51	0.56	0.35				2.65	0.38	29.26	1.06
14	0.55	0.23	2.7	0.32	0.48				2.69	0.37	29.21	1.27
15	0.55	0.23	2.25	0.46	0.40				2.9	0.35	30.12	1.14
16	0.55	0.22	2.41	0.37	0.39				2.41	0.41	30.96	1.39
17	0.54	0.23	2.8	0.35					1.1	0.32	22.76	1.29
18	0.62	0.33	3.9	0.38	0.16		0.79	1.54				
19	0.61	0.43	4.6	0.52	0.20		0.78	1.18				
20	0.56	0.57	4.3	0.69	0.28		0.81	0.69				
21	0.55	0.39	3.8	0.87								
22	0.63	0.51	3.52	0.78								
23	0.62	0.48	3.44	0.88								
24	0.61	0.31	3.2	0.89								
25	0.41	0.6	3.4	0.85								
26	0.67	0.39	3.35	0.87								
27	0.58	0.55	3.12	0.91								
28	0.54	0.58	3.0	0.92								
29	0.54	0.58	2.95	0.85								
30	0.6	0.47	3.1	0.84								
31	0.54	0.42	3.72	0.36	0.31	0.78	0.68	1.12				
32	0.52	0.38	4.05	0.37	0.21	0.75	0.60	1.18	1.9	0.49		
33	0.44	0.33	3.46	0.39	0.22	0.72	0.62	1.40	1.8	0.38		
34	0.53	0.31	4.11	0.42	0.20	0.74	0.61	1.29	1.6	0.50		
35	0.52	0.32	3.98	0.41	0.21	0.75	0.65	1.60	1.71	0.48		
36	0.53	0.76	4.61	1.09	0.89	0.75	0.63	1.25	1.74	0.54	29.64	2.0
37	0.54	0.99	3.99	1.05	1.88	0.88	0.84	1.06	16.62	0.52	38.48	3.34
38	0.56	0.98	4.25	1.19	2.17	0.87	0.83	1.09	17.23	0.55	39.56	3.38
39	0.57	1.06	4.11	1.13	2.16	0.87	0.83	1.09	17.31	0.53	39.44	3.42
40	0.56	1.02	4.25	1.14	2.19	0.87	0.83	1.09	17.87	0.54	39.52	3.34
41	0.68	0.37	3.51	0.73	0.52	0.78	0.68	0.91	1.36	0.53	28.79	1.31
42	0.61	0.53	3.6	0.65	0.53	0.77	0.66	0.92	1.31	0.59	29.32	1.27
43	0.57	0.73	3.55	0.9	0.79	0.81	0.74	0.82				
44	0.56	0.81	2.79	1.49	1.17	0.85	0.81	0.64	1.15	0.64	27.26	1.57
45	0.57	0.62	2.82	1.53	1.18	0.88	0.86	0.95	1.32	0.56	28.86	1.47
46	0.55	0.76	3.06	1.19	1.10	0.86	0.81	0.66	1.09	0.32	27.95	1.55

R1, C₁₉/C₂₃ tricyclic terpanes; R2, C₂₂/C₂₁ tricyclic terpanes; R3, C₂₄/C₂₃ tricyclic terpanes; R4, C₂₆/C₂₅ tricyclic terpanes; R5, C₂₄ tetracyclic terpanes/C₂₆ tricyclic terpanes; R6, Ts/Tm trisnorhopanes; R7, diahopane/hopane; R8, norhopane/hopane; R9, oleanane/hopane; R10, gammacerane/hopane; R11, C₃₂ 22S/(22S + 22R) homohopanes; R12, C₃₅/C₃₄ extended hopanes; R13, %C₂₇ $\alpha\alpha\alpha$ R; R14, %C₂₈ $\alpha\alpha\alpha$ R; R15, %C₂₉ $\alpha\alpha\alpha$ R; R16, C₂₉ 20S/(20S + 20R); R17, C₂₉ $\beta\beta/(\beta\beta + \alpha\alpha)$; R18, C₂₇ diasteranes/regular steranes; R19, %C₃₀ $\alpha\alpha\alpha$ R; R20, steranes/hopanes; R21, tricyclic terpanes/hopanes; R22, $RC = [(0.6) * (1.5 * (2MP + 3MP)) / (PHEN + 9MP + 1MP)] + 0.37$; R23, MPI, methylphenanthrenes index = $[1.5 * (3MP + 2MP)] / (PHEN + 9MP + 1MP)$; R24, DBT/P = DBT/phenanthrene; R25, *n*-C₇/methylcyclohexane; R26, toluene/*n*-C₇; R27, heptane value (H); R28, isoheptane value (I)

^aParameters used in multivariate statistical analysis

et al. 2005). The *m/z* 191 mass chromatograms (Fig. 13) show that the tricyclic terpane distributions and ratios (Table 5) can be used to distinguish the oils. The Suez Rift oil samples from the southern sector oilfields (e.g., Shadwan and Saqqara) show prominent tricyclic terpanes and characteristically high abundance of the C₂₃ homologue as well as the C₁₉–C₃₀ extended series over the higher C₂₇–C₃₅ hopanoids. Abundant tricyclic terpanes is commonly

observed in highly mature crude oils and source rock extracts from marine carbonate and saline lacustrine environments (Zumberge 1987; Mello et al. 1988; de Grande et al. 1993; Peters 2000).

Several tricyclic and tetracyclic terpanes ratios can be used to distinguish between marine, fresh-water lacustrine, terrigenous, and saline lacustrine oils (Aquino Neto et al. 1982; Ourisson et al. 1982; de Grande et al. 1993). The studied oil samples show

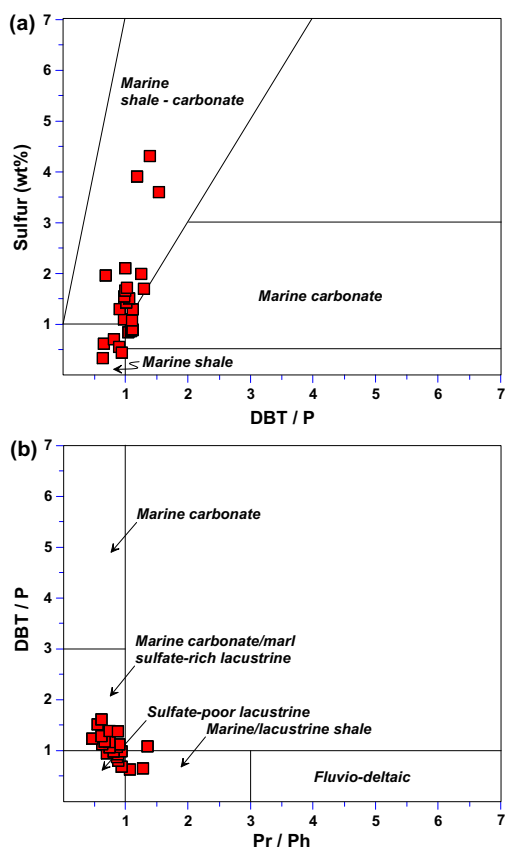


Fig. 14. (a) Relation between dibenzothiophene (DBT)/phenanthrene (P) and sulfur content (% S, wt%), and (b) Pr/Ph versus DBT/P for the Gulf of Suez oils.

a pattern from north to south suggesting spatial differences in the organofacies of the source rock. For example, C_{19}/C_{23} , C_{24}/C_{23} , C_{26}/C_{25} , C_{30} dihopane/hopane, Ts/Tm, oleanane/hopane ratios increase, whereas C_{22}/C_{21} , C_{24} tetracyclic terpane/ C_{26} tricyclic terpane, C_{29} 30-norhopane/hopane ratios decrease, indicating increased higher-plant input, higher thermal maturity, or different redox conditions during source rock deposition (Zumberge 1983; Moldowan et al. 1994; Peters et al. 2005). This finding is supported by plots of dibenzothiophene/phenanthrene (DBT/P) versus sulfur (Fig. 14a) and Pr/Ph versus DBT/P (Fig. 14b; Hughes et al. 1995). Nearly all sampled oils have DBT/P ratios > 1 implying marine marl/carbonate sulfate-rich source rocks with a strong reducing depositional environment. Samples from the Safa, Warda, Edfu, and Saqqara oils in the southern part of the Suez rift have DBT/P ratios < 1 (Table 5), which indicate

that the source rocks for these oils were deposited in a mildly reducing marine shale environment.

One of the prominent features in the Gulf of Suez oils is the presence of high concentrations of gammacerane (Fig. 13; Table 5). Our results show significant abundance of gammacerane in the oil suite, and the gammacerane index is as high as 0.8 (Table 5). The overall low Pr/Ph ratios and the high homohopane indices (C_{35}/C_{34} ratios mostly > 1.0) correlate well with the gammacerane index (Table 5), which make them good indicators for enhanced evaporitic or high-salinity environments accompanied by anoxic deposition conditions (Didyk et al. 1978; Mello et al. 1988; Peters and Moldowan 1991; Sinninghe Damsté et al. 1995) in the Gulf of Suez basin. Rohrback (1983) identified only low concentrations of gammacerane in most of Gulf of Suez oils and concluded that the unusual occurrence of abundant gammacerane in oils from Devonian reservoirs is due to migration-contamination from Carboniferous black shale cap rock.

Relating crude oil biomarkers to organisms whose remains were incorporated into the source rocks is commonly done using sterane ternary diagrams (Fig. 10). The C_{27} - C_{28} - C_{29} steranes ternary diagram (Fig. 10) shows that most of the analyzed oil samples have similar sterane patterns, indicating that they were generated from similar source rocks or different organofacies of the same source rock. The general sterane distribution suggests generation from source rock containing predominantly marine plankton/bacterial-derived organic matter with minor terrigenous input (Seifert and Moldowan 1978; Huang and Meinschein 1979; Moldowan et al. 1985). The high contribution of eukaryotes versus prokaryotes is evidenced by moderate-to-high relative proportions of steranes to hopanes (Table 5). The prevailing marine source rocks is also evidenced by the presence of 24-*n*-propylcholestanes (C_{30} steranes), which are believed to be derived from Chrysophyte algae of Sarcinochrysidales order (Moldowan et al. 1985, 1990).

Thermal Maturity of the Gulf of Suez Oils

In petroleum geochemistry, stereoisomerization or the relative thermal stability of the compounds toward C-C bond cracking is the basic concept of thermal maturity parameters. Biomarker stereoisomerization ratios are among the most useful measures of thermal maturity because biomarkers are

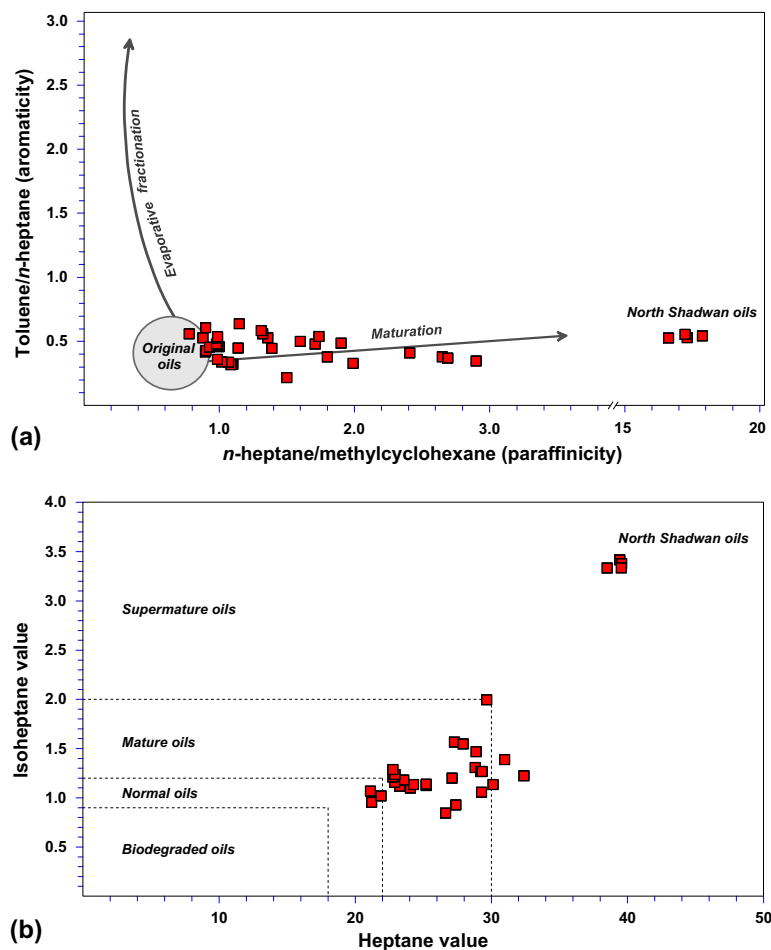


Fig. 15. (a) Aromaticity versus paraffinicity (see Thompson 1987) and (b) heptane value (H%) versus isoheptane value (I%) for crude oil samples from different reservoirs in the central and southern Gulf of Suez Graben (see Thompson 1983).

common in rock extracts and crude oils (Peters et al. 2005).

Numerous saturated and aromatic biomarker ratios can be used to assess thermal maturity of crude oils (Seifert and Moldowan 1979, 1981, 1986; Peters et al. 2005). The most reliable approach to assess thermal maturity of oil is to start based on fast reactions, especially stereoisomer ratios [e.g., C_{32} hopane %22S/(22S + 22R)], followed by slower reactions [e.g., %20S/(20S + 20R) and % $\beta\beta$ /($\beta\beta + \alpha\alpha$) C_{29} steranes], and then followed by the even slower reactions, such as mono- or triaromatic side-chain cleavage ratios.

Nearly all oil samples achieved the C_{32} hopane %22S endpoint (~ 57 – 62%), which represents thermal maturity equivalent to at least the early oil window (Seifert and Moldowan 1986). The Suez oils

have C_{29} sterane %20S/(20S + 20R) ratios of 0.30–0.64 and % $\beta\beta$ /($\beta\beta + \alpha\alpha$) ratios of 0.41–0.68 (Table 5), indicating that the oil samples were generated from source rocks that range from early (~ 0.6 $R_o\%$ for most samples) to the peak of the oil window, which approximately corresponds to ~ 0.8 – 0.9 $R_o\%$ (Fig. 11). It is interesting to note here that some oil samples deviate to the lower right of the maturity curve (Fig. 11), which suggests that secondary migration may cause the enrichment of the % $\beta\beta$ rather than the %20S C_{29} steranes (Seifert and Moldowan 1981).

It is preferable to support the biomarker maturity parameters by additional non-biomarker maturity measurements to corroborate interpretations of oil maturity. Phenanthrenes (P; m/z 178) and methylphenanthrenes (MP; m/z 192) and the

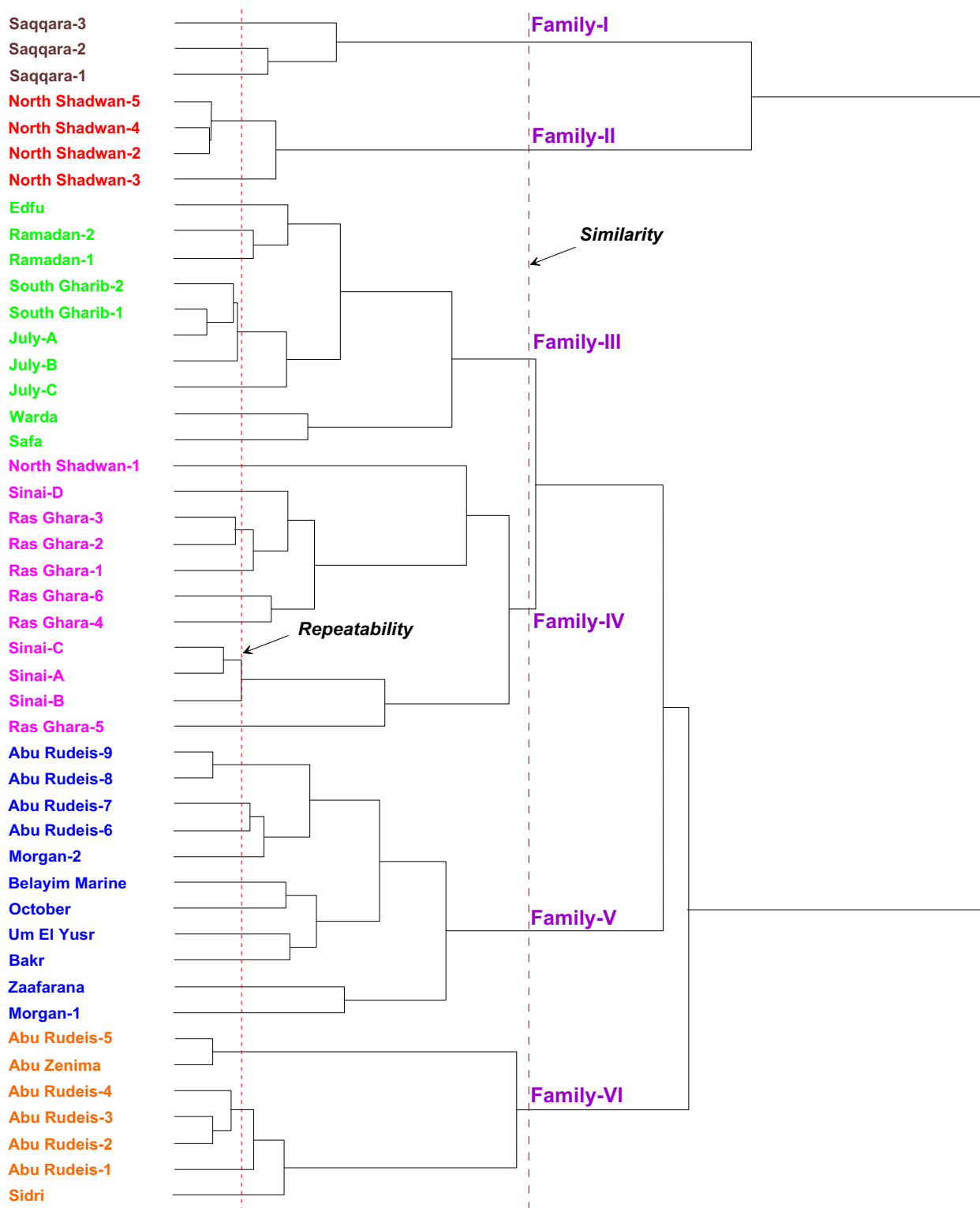


Fig. 16. Hierarchical cluster analysis (HCA) dendrogram identifies six Gulf of Suez oil families based on 16 source-related biomarker ratios. A dashed line of repeatability was established based on two replicate analyses of the Sinai A and Sinai B oil samples.

calculated vitrinite reflectance value (%Rc) based on the methylphenanthrenes index or MPI (Radke and Welte 1983) are the most widely used aromatic maturity parameters. The results from the aromatic maturity parameters correlate with the interpretations based on the biomarker maturity parameters. The MPI values for the samples (0.60–0.86) reveal a wide range of thermal maturity spanning the early to peak oil window where the calculated Rc ranges from 0.72 to 0.88% (Table 5).

Light hydrocarbons are widely used to evaluate reservoir alteration processes, thermal maturity, and oil–oil and oil–condensate correlation (Thompson 1987; Mango 1990; El Diasty 2015). The *n*-heptane/methylcyclohexane (paraffinicity) for most samples is > 1.0 , whereas toluene/*n*-heptane (aromaticity) is fairly low (~ 0.5). Based on the paraffinicity and aromaticity relationships (Table 5; Fig. 15a), none of the Gulf of Suez oils were subjected to in-reservoir evaporative fractionation, but may have experienced secondary changes (i.e., possibly related to maturation or water washing) or prolonged migration. As evidenced earlier from GC and biomarker data, water washing seems an unlikely explanation as none of the oils is biodegraded. Rohrback (1983) suggested that the high *n*-heptane/methylcyclohexane ratios might be due to the high water salinity that reduces oil solubility (Wever 2000). We see that maturation is the major factor that greatly modifies oil variability in the Gulf of Suez; however, migration history and spatial and temporal organofacies variations of the putative source rocks are also included.

Heptane and isoheptane values of Thompson (1987) are sensitive parameters to changes in thermal maturity as they increase with increasing thermal stress. The plot of heptane versus isoheptane indices (Fig. 15b) confirms again the effect of maturity among the Suez Rift oils where the North Shadwan oils (southern sector) plot in the super-mature oil region, consistent with the API and biomarker maturity parameters.

Oil Chemometrics

In this study, we use chemometrics or multivariate statistical analyses (El Diasty et al. 2016; Peters et al. 2016) to evaluate large geochemical data sets to understand, correlate, and classify 46 crude oil samples from the Gulf of Suez into genetic families. Decision tree chemometrics was conducted

Fig. 17. Various biomarker plots; C_{28} vs. C_{29} regular steranes; Ts/Tm trisnorhopanes vs. diahopane/hopane; C_{27} diasteranes/regular steranes vs. diahopane/hopane; % C_{30} steranes vs. oleanane/hopane; gammacerane/hopane vs. C_{27} diasteranes/regular steranes; C_{22}/C_{21} vs. C_{24}/C_{23} tricyclic terpanes; C_{19}/C_{23} tricyclic terpanes vs. C_{24} tetracyclic terpanes/ C_{26} tricyclic terpanes; and C_{27} regular steranes vs. steranes/hopanes for the six Gulf of Suez oil families.

using 16 source-related biomarker ratios, including; C_{19}/C_{23} , C_{22}/C_{21} , C_{24}/C_{23} , C_{26}/C_{25} tricyclic terpanes; C_{24} tetracyclic terpane/ C_{26} tricyclic terpane; Ts/Tm; diahopane/hopane; C_{29} 30-norhopane/hopane; oleanane/hopane; gammacerane/hopane; steranes/hopanes; % C_{27} , % C_{28} , % C_{29} $\alpha\alpha\alpha$ R-steranes; C_{30} steranes; and the C_{27} diasterane/regular sterane ratios. A dashed line of repeatability was established for Figure 16 based on two replicate analyses of the Sinai oil samples (Sinai B and Sinai C; Table 5). Six oil families were identified in the Gulf of Suez basin (Figs. 16, 17, and 18a). Key biomarker parameters used to distinguish different oil families are summarized in Tables 4, 5. The chemometric differentiations based on the biomarker parameters that depict each oil family are defined below.

Family I contains three oil samples from the Saqqara oilfield (Figs. 16, 17). The Saqqara oil family is distinct from the other oil families and shows relatively low sulfur content (0.34–0.62 wt%) and high API gravity (38.4°–41.3°), which may indicate high thermal maturity. High maturity is also indicated by high %20S and % $\beta\beta$ C_{29} steranes isomerization ratios of 0.49–0.54 and 0.55–0.57, respectively. This oil family contains more higher-plant and more angiosperm input based on high C_{19} tricyclic terpane, high oleanane ratios (0.13–0.15), and low C_{30} steranes. The tricyclic terpanes are more abundant than the pentacyclic terpanes. Other biomarker ratios include elevated Pr/Ph (0.91–1.28), DBT/P = 0.64–0.95, canonical variable = -0.02 to -0.56 , high diahopane/hopane, Ts/Tm, diasteranes/regular steranes (Fig. 17), which indicates marine shale source rock with more catalytic clays (see Soffer 1984; Hughes et al. 1995).

The oil samples from the Matulla reservoir in the North Shadwan oilfield belong to Family II group. This oil group shows very high thermal maturity based on light hydrocarbon data, such as high paraffinicity ratios (up to 17.87), heptane and isoheptane values (38.48–39.56 and 3.34–3.42, respectively), moderate-to-high API gravities (25.5°–36.4°), and moderate sulfur content (0.87–

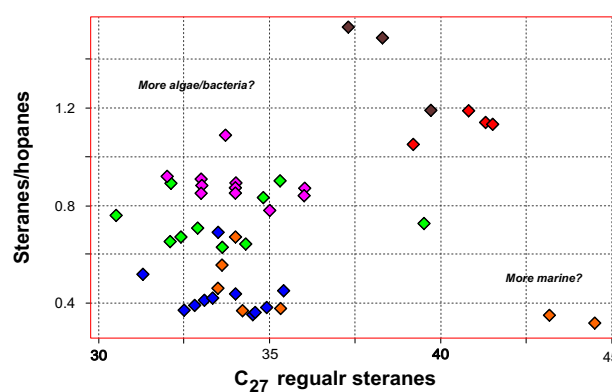
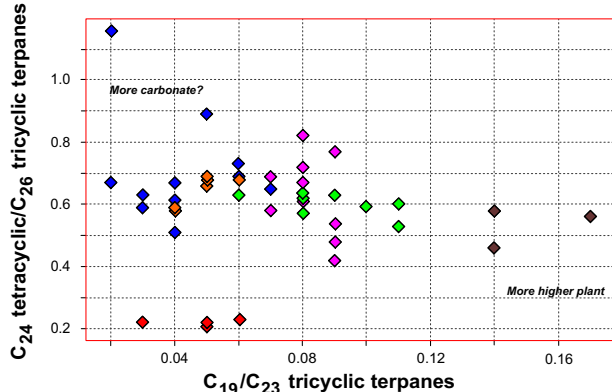
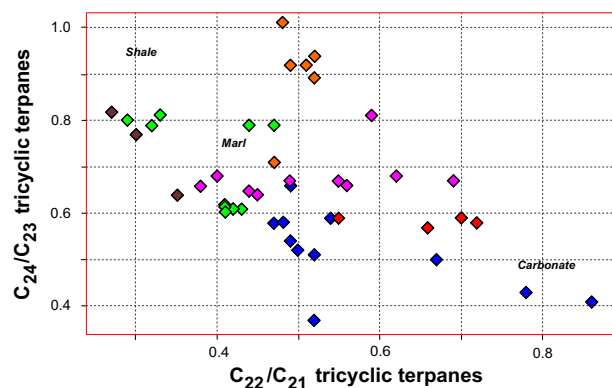
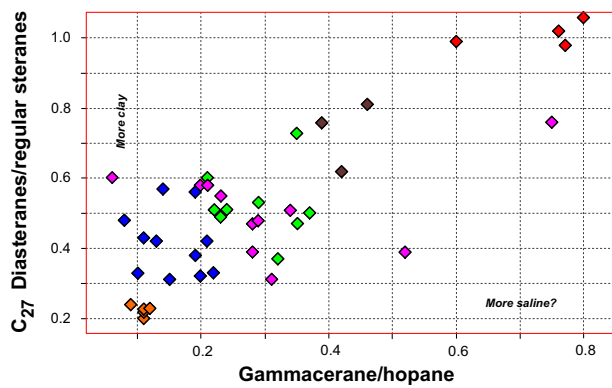
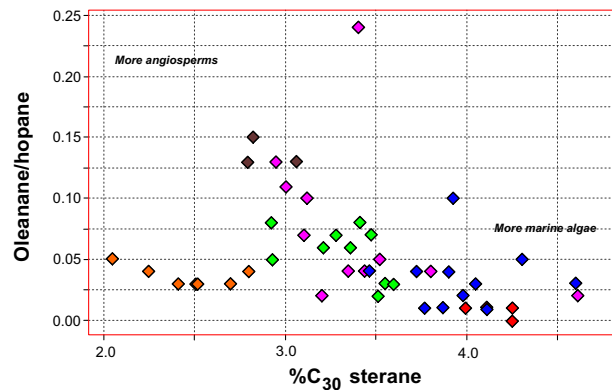
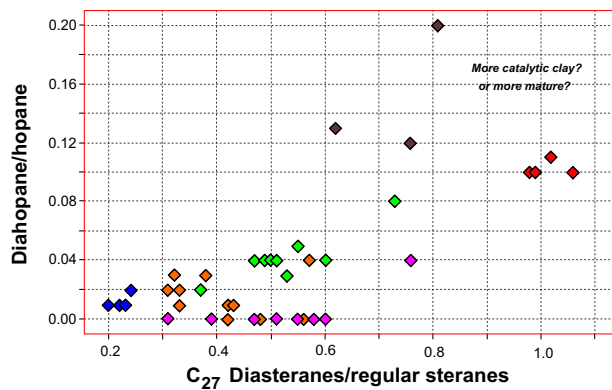
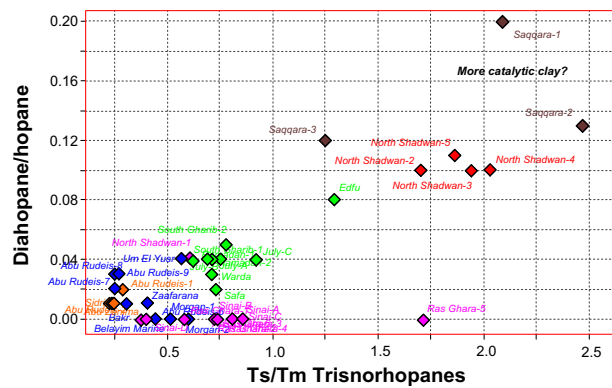
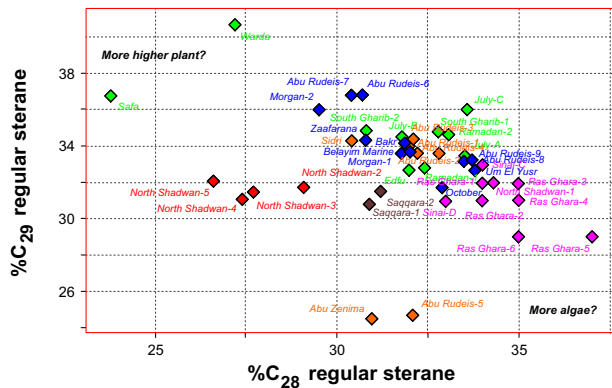




Fig. 18. (a) 3D view of principal component analysis (PCA) identifies oil families in the Gulf of Suez basin and (b) outlier diagnostics plot based on sample residual and Mahalanobis distance to emphasize confidence in the oil classifications. The oil samples are color-coded by family.

Table 6. InStep report for oil–source correlation in the Gulf of Suez Rift basin

No.	Field	Depth (m)	Formation	Category	Classification
1	Geisum	1210	Belayim	0	Not classified
2	Amal	1862	Belayim	0	Not classified
3	Morgan	2408	Rudeis	2	Family II fair match
4	North Shadwan	3347	Rudeis	5	Family V fair match
5	Ras Ghara	3400	Rudeis	4	Family IV fair match
6	Ras Ghara	3415	Rudeis	2	Family II fair match
7	Ras Ghara	3465	Rudeis	3	Family III fair match
8	Ras Ghara	3520	Rudeis	3	Family III fair match
9	Belayim Land	4050	Rudeis	0	Not classified
10	Ras Ghara	2010	Nukhul	5	Family V good match
11	Ras Ghara	2016	Nukhul	5	Family V fair match
12	Ras Ghara	2169	Nukhul	5	Family V fair match
13	Geisum	2316	Nukhul	2	Family II fair match
14	Ras Ghara	3615	Nukhul	2	Family II fair match
15	Amer	948	Thebes	5	Family V good match
16	Amal	2716	Thebes	5	Family V fair match
17	Sinai	3090	Thebes	4	Family IV fair match
18	Morgan	3094	Thebes	2	Family II fair match
19	October	3139	Thebes	5	Family V good match
20	Belayim Marine	3210	Thebes	5	Family V good match
21	Belayim Marine	3216	Thebes	5	Family V good match
22	July	3502	Thebes	2	Family II fair match
23	SB 276	3871	Thebes	3	Family III good match
24	Geisum	2560	Esna	4	Family IV good match
25	Sinai	3100	Esna	5	Family V good match
26	Amer	1149	Br. LS	4	Family IV fair match
27	Ras Ghara	2208	Br. LS	5	Family V fair match
28	Geisum	2682	Br. LS	3	Family III good match
29	Amal	2807	Br. LS	2	Family II fair match
30	Sinai	3120	Br. LS	5	Family V fair match
31	October	3554	Br. LS	5	Family V good match
32	July	3566	Br. LS	2	Family II fair match
33	October	3590	Br. LS	2	Family II fair match
34	North Shadwan	3669	Br. LS	5	Family V fair match
35	SB 276	4081	Br. LS	3	Family III fair match
36	Belayim Land	4722	Br. LS	2	Family II fair match
37	Sinai	3180	Matulla	5	Family V fair match
38	North Shadwan	3749	Matulla	2	Family II fair match
39	SB 276	4124	Matulla	3	Family III fair match

0.94). High diahopane/hopane, Ts/Tm, diasteranes/steranes, and little or no oleanane (Table 5; Fig. 17) suggest clay-rich source rocks or highly mature oils. The tricyclic terpanes are more abundant than pentacyclic terpanes but less than the case of Family I oil. The low Pr/Ph ratios (0.74–0.76, except 1.36 for North Shadwan-4; 3890 m), very high gammacerane indices (0.60–0.80), high C_{35}/C_{34} homohopanes (1.39–1.80), $DBT/P = 1.06–1.09$, $CV = -0.35$ to -0.12 indicate hypersaline anoxic conditions with sulfate-rich marine carbonate or mixed source rocks.

Eight oil samples from Edfu, Ramadan, South Ghariib, and July fields are classified as Family III and two oil samples from Warda and Safa are a

subfamily. Family III oil has intermediate clay content with lower thermal maturity than Family II oil based on moderate diahopane/hopane, Ts/Tm, diasteranes/regular steranes, and higher terrigenous plant input ($\%C_{29}$). Other important bulk and biomarker characteristics that distinguish Family III from other families (Figs. 16, 17) include moderate API (23° – 35°), high sulfur (1.09–1.69 wt%, except for Warda and Edfu: 0.53–0.71 wt%), low Pr/Ph (0.75–0.89), $DBT/P = 0.82–1.11$; and $CV = -1.32$ to 0.23 , which suggest sulfate-rich marine carbonate or mixed source rock facies (Fig. 17).

In spite of different reservoir formations (Matulla, Nukhul, Rudeis, and Kareem), Family IV oils

from Ras Ghara and Sinai oilfields, in addition to North Shadwan-1 oil sample, are substantially similar to each other and different from other oils. Family IV oils have the highest C_{28} sterane content (33–37%). However, Family IV oils have widely varying source biomarker signatures (Table 5; Figs. 16, 17). For example, these oils are characterized by light isotopic ratios (-30.1 to -27.7 for $\delta^{13}C_{Sat}$), whereas the anomalous sample from Kareem oil reservoir (3044–3084 m) from the Ras Ghara-5 well (Fig. 7) is characterized by heavy carbon isotopic values (-24.5‰ for $\delta^{13}C_{Sat}$ and -22.6‰ for $\delta^{13}C_{Aro}$). Family IV oils have Pr/Ph ratios mostly < 1.0 , low-to-moderate oleanane content (0.02–0.13), high gammacerane (> 0.2) and predominance of homohopane series. These geochemical characteristics pinpoint to derivation from algal and terrigenous organic matter deposited under suboxic–anoxic hypersaline shaly source rocks not older than the Late Cretaceous. Oil from Ras Ghara-5 has low amounts of tricyclic terpanes, high isoprenoid ratio (Pr/Ph = 1.37), high diasteranes and oleananes (> 0.20), near absence of gammacerane, and high diasteranes and diahopanes. These features point to an origin from a Tertiary clay-rich source rock deposited under suboxic–anoxic non-hypersaline depositional settings.

Family V includes 11 oil samples from the Abu Rudeis, Morgan, Belayim Marine, October, Um El Yusr, and Bakr in the central part of the Gulf of Suez (Fig. 1), and Zaafarana and Morgan-1 samples were identified as a separate subfamily. This oil family has relatively low API gravity (12° – 27°) and high to very high sulfur (1.66–4.31 wt%). The low Pr/Ph (0.59–0.94), moderate-to-high DBT/P (0.69–1.60), and canonical variable ($CV = -1.32$ to -0.03) are consistent with anoxic marine carbonate/marl facies source rocks. These source rocks are clay-poor based on low diahopane/hopane, Ts/Tm and diasteranes/steranes, and more marly character (elevated C_{24} tetracyclic terpanes and high C_{22}/C_{21} tricyclic terpanes).

With the Matulla as the principal reservoir, in addition to Nubia, Thebes, and Nukhul reservoirs, oil samples from Abu Rudeis (1–5) Abu Zenima and Sidri oilfields are linked to Family VI. This oil family resembles Family V where API gravity is low (12.8° – 22.6°), with high sulfur (1.05–3.69 wt%), and low Pr/Ph (0.49–0.73). The common features of the environment of deposition of source rocks for this oil family include, low clay (low diahopane/hopane, Ts/Tm, diasteranes/regular steranes), shaly (high $C_{24}/$

C_{23} , low or no oleanane, and C_{30} steranes), and unstratified water column (low gammacerane/hopane, C_{35}/C_{34} homohopanes), which are consistent with a marine carbonate environment.

Figure 18b shows an outlier diagnostics plot based on sample residual and Mahalanobis distance. In this figure, the samples are color-coded by family. The two black lines divide the plot into four quadrants. Samples in the lower left quadrant (nearly all samples) show PCA results that are well behaved and none are outliers. The quadrant at upper right contains no samples. If it did, those samples would clearly be outliers and their classification would be problematic. A few samples (i.e., Ras Ghara-5, North Shadwan-1, Zaafarana, and Abu Zenima oils) in the quadrant at lower right fall within acceptable values of sample residual, but are outside the Mahalanobis distance that would indicate acceptable classification. These samples might be considered outliers, but their classification is likely acceptable.

Oil–Source Correlation

The genetic relationship between recovered hydrocarbons and probable source rocks is the critical link to establish the petroleum systems in mature rift systems (Katz 1995; El Diasty et al. 2014, 2017a). Oil-to-source rock correlation is a more difficult task than oil–oil correlation (Hunt 1996) for multiple reasons: (1) a few samples cannot adequately represent oil generated from a thick source interval having varying character; (2) throughout their generation history, source rocks do not yield oil of the same composition; and (3) the composition of the bitumen from the rock is not necessarily the same in the fine pores of the rock matrix as it is in the micro-fractures and bedding planes.

Based on screening analyses, molecular and isotopic characteristics of the oils, and the above-mentioned source rock extracts, a positive oil–source correlation seems to be evident between them and indicates that the Gulf of Suez oils likely incorporate contributions from the Campanian (Brown Limestone), Paleocene (Esna), Eocene (Thebes), and Lower Miocene (Nukhul) formations. Carbon isotope ratios of the saturated and aromatic fractions from extractable rock bitumen are similar to those of the Gulf of Suez oils in Figure 6.

Gas chromatographic distributions and isoprenoid branched hydrocarbons also provide evi-

dence for correlation purposes. The *n*-alkane distributions and isoprenoid ratios for extracts from different source rock intervals show good correlation with the Gulf of Suez oils (Fig. 9). Likewise, comparison of the sterane distributions of the extracts with that of the oils (Fig. 10) indicates similar marine plankton/bacterial organic matter and nearly identical source rock depositional environments. The overall geochemical similarity between the Gulf of Suez oils and the analyzed source rocks confirms the mixed nature of these fluids and suggests that no single source rock horizon is responsible for the oil. Although immature in some cases, most of the rock samples show sufficient maturity to be active source rocks for the oil generation (Fig. 11).

Oil–source correlation in the Gulf of Suez can be significantly improved using a more advanced tool that can manage many source variables and find the best fit between candidate source rocks and the oil samples.

Table 6 shows the InStep report from the watched folder consisting of six columns. Column 2 lists the extract samples; the “category” or family designation is in column 5 with the degree of fit in column 6. Additional information is given in columns 1, 3, and 4. The results of the analyses include seven “good” fits of extracts to oil Family V (central Gulf of Suez), two “good” fits to oil Family III (northern south Gulf of Suez), and one “good” fit to oil Family IV (eastern south Gulf of Suez; Table 6). This means that, of all the stratigraphic units studied in the Gulf of Suez, the bulk of evidence points to the Brown Limestone, Esna, Thebes, and Nukhul formations as the best candidate source rocks for Family III, Family IV, and Family V oils (Table 6). Interestingly, none of the rock extracts classify as Family I (western south Gulf of Suez) or Family VI (eastern central Gulf of Suez). Because there are so few samples in some of the categories (especially Family I), the SIMCA model has only two factors, a setting that could yield some failed classifications of future data because of the lack of information built into the model. “Fair” matches are less likely to be valid.

Finally, the Gulf of Suez is a reasonably mature basin and still awaiting renewal with either state-of-the-art seismic imaging, or, ultimately, the development of unconventional plays in the organically rich stratigraphic intervals of the Thebes and Brown Limestone.

CONCLUSIONS

One hundred and twenty-three Upper Cretaceous—Lower Miocene source rocks and 46 crude oil samples from the Gulf of Suez Rift basin were selected for detailed bulk geochemical, biomarker, and stable carbon isotopic analyses in order to differentiate oil families using chemometrics and establish genetic relationships between oils and various petroleum source units. The main results of the study are outlined below:

- The Gulf of Suez contains several organic-rich intervals, but the pre-rift Brown Limestone and Thebes source rock samples contain very good-to-excellent organic content. However, the Miocene rocks are rated fair to good where the sedimentary environment has been less favorable for preservation of organic material.
- HI and T_{\max} pyrolysis data indicate variable kerogen type and maturation histories in different parts of the Suez Rift basin, which are related to differences in organic facies, paleo-heat flow, and lithology-related heat conductivity and heat capacity. The vast majority of the analyzed samples fall along the Type II and Type II/III kerogen maturation paths with a few samples falling within the Type I or Type III kerogen maturation pathways.
- Alkane and aromatic hydrocarbon fractions yield carbon isotope and biomarker ratios in the bitumen samples that indicate predominantly anoxic conditions and substantial algal/bacterial marine-derived organic matter with minor terrigenous input to the source rocks. Abundant gammacerane implies deposition in stratified saline to hypersaline anoxic water with significant halophilic bacterial input to these sediments.
- Maturity-related parameters show that most of the Gulf of Suez source rocks were not buried deeper than the early oil generation window and generally the extract samples vary from immature to the main stage of oil window with $\%R_o < 0.9$.
- The Gulf of Suez oils exhibit a wide range of chemical composition from heavy-to-medium API gravity and moderate-to-high sulfur content. The quantity of sulfur decreases systematically with increasing oil gravity from

north to south, consistent with greater crustal extension and thermal subsidence of the southern sector compared to the central and northern provinces of the Suez Rift.

- Based on stable carbon isotope compositions, *n*-alkanes, isoprenoids, and sterane and terpane biomarkers, the Gulf of Suez oils were derived from carbonate/marl source rocks rich in phytoplankton/benthic algae and bacterial organic matter with fair contribution of terrigenous organic debris, deposited under anoxic conditions with different thermal maturity histories equivalent to at least the early oil window.
- Chemometric analysis using 16 source-related biomarker and isotope ratios for 46 oil samples identifies six genetic families in the Gulf of Suez basin. The oil families share common characteristics where the precursor organic matter deposited in a restricted marine environment where the contribution of land-derived organic matter is limited. Thermal maturation is a major factor that accounts for variable compositions among the Gulf of Suez oil families. However, migration history and spatial and temporal organofacies variations of the putative source rocks are also included.
- The overall geochemical similarity between the Gulf of Suez oils and the analyzed source rocks confirms the mixed nature of these fluids and suggests that no single source rock horizon is likely to have sourced the oil in this promising rift basin. Based on oil–source correlation and an InStep chemometric decision tree model, the Brown Limestone, Esna, Thebes, and Nukhul formations are the effective source rocks for Family III, Family IV, and Family V oils, whereas none of the source rock extracts has been assigned for Family I or Family VI oils.

ACKNOWLEDGMENTS

The authors thank John and Alex Zumberge (GeoMark Research, Ltd. Houston, TX) for providing essential data, facilitating rock and oil analyses, and technical assistance during the course of this project. Some of the screening and biomarker

analyses on rock extracts and oils were conducted at the Department of Applied Geosciences and Geophysics, Montanuniversität Leoben, Austria, and StratoChem Services, Cairo. We thank Mike Moldovan (Biomarker Technologies Inc., CA), the Editor-in-Chief John Carranza, and two anonymous reviewers for their comments that greatly improved the quality of manuscript.

REFERENCES

- Alizadeh, B., Alipour, M., Chehrazi, A., & Mirzaie, S. (2017). Chemometric classification and geochemistry of oils in the Iranian sector of the southern Persian Gulf Basin. *Organic Geochemistry*, *111*, 67–81.
- Alsharhan, A. S. (2003). Petroleum geology and potential hydrocarbon plays in the Gulf of Suez rift basin, Egypt. *American Association of Petroleum Geologists Bulletin*, *87*(1), 143–180.
- Alsharhan, A. S., & Salah, M. G. (1994). Geology and hydrocarbon habitat in a rift setting: southern Gulf of Suez, Egypt. *Bulletin of Canadian Petroleum Geology*, *42*(3), 312–331.
- Alsharhan, A. S., & Salah, M. G. (1995). Geology and hydrocarbon habitat in rift setting: northern and central Gulf of Suez, Egypt. *Bulletin of Canadian Petroleum Geology*, *43*(2), 156–176.
- Alsharhan, A. S., & Salah, M. G. (1997). A common source rock for Egyptian and Saudi hydrocarbons in the Red Sea. *American Association of Petroleum Geologists Bulletin*, *81*(10), 1640–1659.
- Angelier, J. (1985). Extension and rifting: the Zeit region, Gulf of Suez. *Journal of Structural Geology*, *7*(5), 605–612.
- Aquino Neto, F. R., Restlé, A., Connan, J., Albrecht, P., & Ourisson, G. (1982). Novel tricyclic terpanes (C₁₉, C₂₀) in sediments and petroleum. *Tetrahedron Letters*, *23*, 2027–2030.
- Aquino Neto, F. R., Trendel, J. M., Restle, A., Connan, J., & Albrecht, P. A. (1983). Occurrence and formation of tricyclic and tetracyclic terpanes in sediments and petroleum. In M. Bjørøy, C. Albrecht, & C. Cornford (Eds.), *Advance in organic geochemistry 1981* (pp. 659–676). New York: Wiley.
- Bakr, M. Y., & Wilkes, H. (2002). The influence of facies and depositional environment on the occurrence and distribution of carbazoles and benzocarbazoles in crude oils: a case study from the Gulf of Suez, Egypt. *Organic Geochemistry*, *33*, 561–580.
- Barakat, A. O., Mostafa, A., El-Gayar, M. S., & Rullkötter, J. (1997). Source-dependent biomarker properties of five crude oils from the Gulf of Suez, Egypt. *Organic Geochemistry*, *26*, 441–450.
- Barakat, A. O., Mostafa, A. R., Qian, Y., Kim, M., & Kennicutt, M. C., II. (2005). Organic geochemistry indicates Gebel El Zeit, Gulf of Suez is a source of bitumen used in some Egyptian mummies. *Geoarchaeology*, *20*(3), 211–228.
- Béhar, F., Beaumont, V., & Penteadó, H.L. De B. (2001). Rock-Eval 6 technology: Performances and developments. *Oil and Gas Science and Technology*, *56*(2), 111–134.
- Bosence, D. (2012). Carbonate-dominated marine rifts. In D. G. Roberts & A. W. Bally (Eds.), *Regional geology and tectonics: Phanerozoic rift systems and sedimentary basins* (pp. 105–130). Amsterdam: Elsevier.
- Bosworth, W. (1985). Geometry of propagating continental rifts. *Nature*, *316*(15), 625–627.

- Bosworth, W. (1995). A high-strain rift model for the southern Gulf of Suez (Egypt). In J. J. Lambaise (Ed.), *Hydrocarbon habitat in rift basins* (Vol. 80, pp. 75–112). London: Geological Society of London, Special Publication.
- Bosworth, W. (2015). Geological evolution of the Red Sea: Historical background, review, and synthesis. In N. M. A. Rasul & I. C. F. Stewart (Eds.), *The Red Sea* (pp. 45–78). Berlin: Springer.
- Bosworth, W., Crevello, P., Winn, R. D., Jr., & Steinmetz, J. (1998). Structure, sedimentation, and basin dynamics during rifting of the Gulf of Suez and northwestern Red Sea. In B. H. Purser & D. W. J. Bosence (Eds.), *Sedimentation and tectonics of rift basins: Red Sea-Gulf of Aden* (pp. 77–96). London: Chapman and Hall.
- Bosworth, W., & Durocher, S. (2017). Present-day stress fields of the Gulf of Suez (Egypt) based on exploratory well data: Non-uniform regional extension and its relation to inherited structures and local plate motion. *Journal of African Earth Sciences*, 136, 136–147.
- Bosworth, W., Khalil, S., Clare, A., Comisky, J., Abdelal, H., Reed, T., et al. (2014). Integration of outcrop and subsurface data during the development of a naturally fractured Eocene carbonate reservoir at the East Ras Budran concession, Gulf of Suez, Egypt. In G. H. Spence, J. Redfern, R. Aguilera, T. G. Bevan, J. W. Cosgrove, G. D. Couples, & J.-M. Daniel (Eds.), *Advances in the study of fractured reservoirs* (Vol. 374, pp. 333–359). London: Geological Society of London, Special Publications.
- Bosworth, W., & McClay, K. (2001). Structural and stratigraphic evolution of the Gulf of Suez rift, Egypt: A synthesis. In P. A. Ziegler, W. Cavazza, A. H. F. Robertson, & S. Crasquin-Soleau (Eds.), *Peri-Tethys Memoir 6: Peri-Tethyan Rift/Wrench Basins and Passive Margins* (Vol. 186, pp. 567–606). Paris: Memoires du Muséum National d'Histoire Naturelle de Paris.
- Bosworth, W., & Stockli, D. F. (2016). Early magmatism in the greater Red Sea rift: timing and significance. *Canadian Journal of Earth Sciences*, 53, 1–19.
- Brassell, S. C., Sheng, G., Fu, J., & Eglinton, G. (1988). Biological markers in lacustrine Chinese oil shales. In A. J. Fleet, K. Kelts, & M. R. Talbot (Eds.), *Lacustrine petroleum source rocks* (Vol. 40, pp. 299–308). London: Geological Society of London, Special Publication.
- Carvajal-Ortiz, H., & Gentzis, T. (2015). Critical considerations when assessing hydrocarbon plays using Rock-Eval pyrolysis and organic petrology data: Data quality revisited. *International Journal of Coal Geology*, 152, 113–122.
- Clark, J. P., & Philp, R. P. (1989). Geochemical characterization of evaporite and carbonate depositional environments and correlation of associated crude oils in the Black Creek Basin, Alberta. *Bulletin of Canadian Petroleum Geology*, 37, 401–416.
- Colletta, B., Le Quellec, P., Letouzy, J., & Moretti, I. (1988). Longitudinal evolution of the Suez rift structure (Egypt). *Tectonophysics*, 153, 221–233.
- Collister, J. W., & Wavrek, D. A. (1996). $\delta^{13}\text{C}$ compositions of saturate and aromatic fractions of lacustrine oils and bitumens: Evidence for water column stratification. *Organic Geochemistry*, 24, 913–920.
- Connan, J., & Cassou, A. M. (1980). Properties of gases and petroleum liquids derived from terrestrial kerogen at various maturation levels. *Geochimica et Cosmochimica Acta*, 44(1), 1–23.
- Cornford, C., Gardner, P., & Burgess, C. (1998). Geochemical truths in large data sets. I: Geochemical screening data. *Organic Geochemistry*, 29(1–3), 519–530.
- Dahl, J. E., Moldowan, J. M., Teerman, S. C., McCaffrey, M. A., Sundararaman, P., & Stelting, C. E. (1994). Source rock quality determination from oil biomarkers I: A new geochemical technique. *American Association of Petroleum Geologists Bulletin*, 78, 1507–1526.
- Darwish, M., & El-Araby, A. M. (1993). Petrography and diagenetic aspects of some siliciclastic hydrocarbon reservoirs in relation to the rifting of the Gulf of Suez. In E. Philobos & B. H. Purser (Eds.), *Geodynamics and sedimentation of the Red Sea-Gulf of Aden Rift System* (Vol. 1, pp. 155–189). Geological survey of Egypt: Special Publication.
- de Grande, S. M. B., Aquino Neto, F. R., & Mello, M. R. (1993). Extended tricyclic terpanes in sediments and petroleum. *Organic Geochemistry*, 20(7), 1039–1047.
- Dembicki, H., Jr. (2009). Three common source rock evaluation errors made by geologists during prospect or play appraisals. *American Association of Petroleum Geologists Bulletin*, 93, 341–356.
- Didyk, B. M., Simoneit, B. R. T., Brassell, S. C., & Eglinton, G. (1978). Organic geochemical indicators of palaeoenvironmental conditions of sedimentation. *Nature*, 272, 216–222.
- El Atfy, H., Brocke, R., Uhl, D., Ghassal, B., Stock, A. T., & Littke, R. (2014). Source rock potential and paleoenvironment of the Miocene Rudeis and Kareem formations, Gulf of Suez, Egypt: An integrated palynofacies and organic geochemical approach. *International Journal of Coal Geology*, 131, 326–343.
- El Diasty, W. Sh. (2015). Khatatba Formation as an active source rock for hydrocarbons in the northeast Abu Gharadig Basin, north Western Desert, Egypt. *Arabian Journal of Geosciences*, 8(4), 1903–1920.
- El Diasty, W. Sh., El Beialy, S. Y., Abo Ghonaim, A. A., Mostafa, A. R., & El Atfy, H. (2014). Palynology, palynofacies and petroleum potential of the Upper Cretaceous-Eocene Matulla, Brown Limestone and Thebes formations, Belayim oilfields, central Gulf of Suez, Egypt. *Journal of African Earth Sciences*, 95, 155–167.
- El Diasty, W. Sh., El Beialy, S. Y., Anwari, T. A., Peters, K. E., & Batten, D. J. (2017a). Organic geochemistry of the Silurian Tanezzuft Formation and crude oils, NC115 Concession, Murzuq Basin, southwest Libya. *Marine and Petroleum Geology*, 86, 367–385.
- El Diasty, W. Sh., El Beialy, S. Y., El Attar, R. M., Khairy, A., Peters, K. E., & Batten, D. J. (2019). Oil-source correlation in the West Esh El Mellaha, southwestern margin of the Gulf of Suez rift, Egypt. *Journal of Petroleum Science and Engineering*, 180, 844–860.
- El Diasty, W. Sh., El Beialy, S. Y., Mahdi, A. Q., & Peters, K. E. (2016). Geochemical characterization of source rocks and oils from northern Iraq: Insights from biomarker and stable carbon isotope investigations. *Marine and Petroleum Geology*, 77, 1140–1162.
- El Diasty, W. Sh., El Beialy, S. Y., Mostafa, A. R., Abo Ghonaim, A. A., & Peters, K. E. (2015a). Crude oil geochemistry and source rock potential of the Upper Cretaceous-Eocene succession in the Belayim oilfields, Central Gulf of Suez, Egypt. *Journal of Petroleum Geology*, 38(2), 193–215.
- El Diasty, W. Sh., El Beialy, S. Y., Mostafa, A. R., El Adl, H. A., & Batten, D. J. (2017b). Hydrocarbon source rock potential in the southwestern Gulf of Suez graben: Insights from organic geochemistry and palynofacies studies on well samples from the Ras El Bahar Oilfield. *Marine and Petroleum Geology*, 80, 133–153.
- El Diasty, W. Sh., El Beialy, S. Y., Peters, K. E., Batten, D. J., Al-Beyati, F. M., Mahdi, A. Q., et al. (2018). Organic geochemistry of the Middle-Upper Jurassic Naokelekan Formation in the Ajil and Balad oil fields, northern Iraq. *Journal of Petroleum Science and Engineering*, 166, 350–362.
- El Diasty, W. Sh., Moldowan, J. M., Peters, K. E., Essa, G. I., & Hammad, M. M. (2019b). Organic geochemistry of condensates and natural gases in the northwest Nile Delta offshore

- Egypt. *Journal of Petroleum Science and Engineering* (submitted).
- El Diasty, W. Sh., Mostafa, A. R., El Beialy, S. Y., El Adl, H. A., & Edwards, K. J. (2015b). Organic geochemical characteristics of the Upper Cretaceous-Early Paleogene source rock and correlation with some Egyptian mummy bitumen and oil from the southern Gulf of Suez, Egypt. *Arabian Journal of Geosciences*, 8(11), 9193–9204.
- El Diasty, W. Sh., & Peters, K. E. (2014). Genetic classification of oil families in the central and southern sectors of the Gulf of Suez, Egypt. *Journal of Petroleum Geology*, 37, 105–126.
- El-Shafey, M., Birgel, D., El-Kammar, A., El-Barkooky, A., Wagreich, M., Tahoun, S., et al. (2017). Integrated palaeo-environmental proxies of the Campanian to Danian organic-rich Quseir section, Egypt. *Marine and Petroleum Geology*, 86, 771–786.
- Elzarka, M. H., & Mostafa, A. R. (1988). Oil prospects of the Gulf of Suez, Egypt—A case study. *Organic Geochemistry*, 12(2), 109–121.
- Espitalié, J., Deroo, G., & Marquis, F. (1985). La pyrolyse Rock-Eval et ses applications and developments. *Revue de l'Institut Français du Pétrole*, 40, 563–580.
- Espitalié, J., La Porte, J. L., Madec, M., Marquis, F., Le Plat, P., Paulet, J., et al. (1977). Methode rapide de caracterisation des roches meres de leur potentiel petrolier et de leur degre d'evolution. *Revue de l'Institut Français du Pétrole*, 32, 23–42.
- Evans, A. L. (1988). Neogene tectonic and stratigraphic events in the Gulf of Suez rift area. *Egypt. Tectonophysics*, 153, 235–247.
- Garfunkel, Z., & Bartov, Y. (1977). The tectonics of the Suez Rift. *Geological Survey of Israel Bulletin*, 71, 44.
- Grice, K., Schouten, S., Peters, K. E., & Sinninghe Damsté, J. S. (1998). Molecular isotopic characterisation of hydrocarbon biomarkers in Palaeocene-Eocene evaporitic, lacustrine source rocks from the Jiangnan Basin, China. *Organic Geochemistry*, 29, 1745–1764.
- Huang, W.-Y., & Meinschein, W. G. (1979). Sterols as ecological indicators. *Geochimica et Cosmochimica Acta*, 43(5), 739–745.
- Hughes, W. B., Holba, A. G., & Dzou, L. I. P. (1995). The ratios of dibenzothiophene to phenanthrene and pristane to phytane as indicators of depositional environment and lithology of petroleum source rocks. *Geochimica et Cosmochimica Acta*, 59, 3581–3598.
- Hunt, J. M. (1996). *Petroleum geochemistry and geology* (p. 743). New York: Freeman and Company.
- Katz, B. J. (1995). A survey of rift basin source rocks. In J. J. Lambiase (Ed.), *Hydrocarbon habitat in rift basins* (Vol. 80, pp. 213–242). London: Geological Society of London, Special Publication.
- Khalil, S. M., & McClay, K. R. (2001). Tectonic evolution of the NW Red Sea-Gulf of Suez rift system. In R. C. L. Wilson, R. B. Whitmarsh, B. Taylor, & N. Froitzheim (Eds.), *Non-volcanic rifting of continental margins: A comparison of evidence from land and sea* (Vol. 187, pp. 453–473). London: Geological Society of London, Special Publication.
- Khalil, S. M., & McClay, K. R. (2016). 3D geometry and kinematic evolution of extensional fault-related folds, NW Red Sea, Egypt. In C. Childs, R. E. Holdsworth, C. A.-L. Jackson, T. Manzocchi, J. J. Walsh, & G. Yielding (Eds.), *The geometry and growth of normal faults* (Vol. 439, pp. 109–130). London: Geological Society of London, Special Publication.
- Khavari-Khorasani, G., Michelsen, J. K., & Dolson, J. C. (1998). The factors controlling the abundance and migration of heavy vs. light oils, as constrained by data from the Gulf of Suez. Part I: The effect of expelled petroleum composition, PVT properties and petroleum system geometry. *Organic Geochemistry*, 29, 255–282.
- Kolaczowska, E., Slougui, N. E., Watt, D. S., Maruca, R. E., & Moldowan, J. M. (1990). Thermodynamic stability of various alkylated, dealkylated and rearranged 17 α - and 17 β -hopane isomers using molecular mechanics calculations. *Organic Geochemistry*, 16(4–6), 1033–1038.
- Lafargue, E., Marquis, F., & Pillot, D. (1998). Rock-Eval 6 applications in hydrocarbon exploration, production, and soil contamination studies. *Revue de l'Institut Français du Pétrole*, 53(4), 421–437.
- Lambaise, J. J., & Bosworth, W. (1995). Structural controls on sedimentation in continental rifts. In J. J. Lambaise (Ed.), *Hydrocarbon Habitat in Rift Basins* (Vol. 80, pp. 117–144). London: Geological Society of London, Special Publications.
- Lewan, M. D. (1984). Factors controlling the proportionality of vanadium to nickel in crude oils. *Geochimica et Cosmochimica Acta*, 48, 2231–2238.
- Mackenzie, A. S., & McKenzie, D. (1983). Isomerization and aromatization of hydrocarbons in sedimentary basins formed by extension. *Geological Magazine*, 120, 417–470.
- Mango, F. D. (1990). The origin of light cycloalkanes in petroleum. *Geochimica et Cosmochimica Acta*, 54(1), 23–27.
- McClay, K. R., Nichols, G. J., Khalil, S. M., Darwish, M., & Bosworth, W. (1998). Extensional tectonics and sedimentation, eastern Gulf of Suez, Egypt. In B. H. Purser & D. W. J. Rodence (Eds.), *Sedimentation and tectonics in rift basins: Red Sea—Gulf of Aden* (pp. 211–238). London: Chapman Hall.
- Mello, M. R., Telneas, N., Gaglianone, P. C., Chicarelli, M. J., Brassell, S. J., & Maxwell, J. R. (1988). Organic geochemical characterization of depositional paleoenvironments of source rocks and oils in Brazilian marginal basins. *Organic Geochemistry*, 13, 31–45.
- Moldowan, J. M., Dahl, J., Huizinga, B. J., Fago, F. J., Hickey, L. J., Peakman, T. M., et al. (1994). The molecular fossil record of oleanane and its relation to angiosperms. *Science*, 265, 768–771.
- Moldowan, J. M., Fago, F. J., Carlson, R. M. K., Young, D. C., Van Duyne, G., Clardy, J., et al. (1991). Rearranged hopanes in sediments and petroleum. *Geochimica et Cosmochimica Acta*, 55, 3333–3353.
- Moldowan, J. M., Fago, F., Lee, C. Y., Jacobson, S. R., Watt, D. S., Slougui, N., et al. (1990). Sedimentary 24-n-propylcholestanes, molecular fossils diagnostic of marine algae. *Science*, 247, 309–312.
- Moldowan, J. M., Seifert, W. K., & Gallegos, E. J. (1985). Relationship between petroleum composition and depositional environment of petroleum source rocks. *American Association of Petroleum Geologists Bulletin*, 69, 1255–1268.
- Moldowan, J. M., Sundaraman, P., & Schoell, M. (1986). Sensitivity of biomarker properties to depositional environment and/or source input in the Lower Toarcian of SW-Germany. *Organic Geochemistry*, 10, 915–926.
- Moretti, I., & Chénet, P. Y. (1987). The evolution of the Suez rift: a combination of stretching and secondary convection. *Tectonophysics*, 133, 229–234.
- Moretti, I., & Colletta, B. (1987). Spatial and temporal evolution of the Suez Rift subsidence. *Journal of Geodynamics*, 7, 151–168.
- Morley, C. K., Nelson, R. A., Patton, T. L., & Munn, S. G. (1990). Transfer zones in the East African Rift System and their relevance to hydrocarbon exploration in rifts. *American Association of Petroleum Geologists Bulletin*, 74(8), 1234–1253.
- Mostafa, A. R. (1993). Organic geochemistry of source rocks and related crude oils in the Gulf of Suez. *Egypt. Berliner Geowissenschaftliche Abhandlungen, A*, 147, 163.
- Mostafa, A. R. (1999). Organic geochemistry of the Cenomanian-Turonian sequence at Bakr Area, Gulf of Suez. *Egypt. Petroleum Geoscience*, 5, 43–50.

- Moustafa, A. M. (1976). Block faulting in the Gulf of Suez. In *Proceedings of the 5th Egyptian General Petroleum Corporation Exploration Seminar* (p. 35).
- Moustafa, A. R. (2002). Controls on the geometry of transfer zones in the Suez rift and northwest Red Sea: Implications for the structural geometry of rift systems. *American Association of Petroleum Geologists Bulletin*, 86(6), 979–1002.
- Moustafa, A. R., & Khalil, H. M. (1995). Superposed deformation in the northern Suez Rift, Egypt: relevance to hydrocarbons exploration. *Journal of Petroleum Geologists*, 18(3), 245–266.
- Mukhopadhyay, P. K., Wade, J. A., & Kruge, M. A. (1995). Organic facies and maturation of Jurassic/Cretaceous rocks, and possible oil-source rock correlation based on pyrolysis of asphaltenes, Scotian Basin, Canada. *Organic Geochemistry*, 22, 85–104.
- Ourisson, G., Albrecht, P., & Rohmer, M. (1984). The microbial origin of fossil fuels. *Scientific American*, 251(2), 44–51.
- Ourisson, G., Albrecht, P., & Rohmer, M. (1982). Predictive microbial biochemistry from molecular fossils to procaryotic membranes. *Trends in Biochemical Sciences*, 7, 236–239.
- Palacas, G. P., Anders, D. E., & King, J. D. (1984). South Florida Basin—A prime example of carbonate source rocks of petroleum. In J. G. Palacas (Ed.), *Petroleum geochemistry and source rock potential of carbonate rocks* (Vol. 18, pp. 71–96). Tulsa: American Association of Petroleum Geologists, Studies Geology.
- Patton, T. L., Moustafa, A. R., Nelson, R. A., & Abdine, S. A. (1994). Tectonic evolution and structural setting of the Suez Rift. In S. M. Landon (Ed.), *Interior rift basins* (Vol. 59, pp. 7–55). Tulsa: American Association of Petroleum Geologists Memoir.
- Peijs, J. A. M. M., Bevan, T. G., & Piombino, J. T. (2012). The Gulf of Suez rift basin. In D. G. Roberts & A. W. Bally (Eds.), *Regional geology and tectonics: Phanerozoic rift systems and sedimentary basins* (pp. 165–194). The Netherlands: Elsevier.
- Peters, K. E. (1986). Guidelines for evaluating petroleum source rock using programmed pyrolysis. *American Association of Petroleum Geologists Bulletin*, 70, 318–329.
- Peters, K. E. (2000). Petroleum tricyclic terpanes: predicted physicochemical behavior from molecular mechanics calculations. *Organic Geochemistry*, 31, 497–507.
- Peters, K. E., & Cassa, M. R. (1994). Applied source rock geochemistry. In L. B. Magoon & W. G. Dow (Eds.), *The petroleum system—from source to trap* (Vol. 60, pp. 93–120). Tulsa: American Association of Petroleum Geologists Memoir.
- Peters, K. E., Coutrot, D., Nouvelle, X., Ramos, L. S., Rohrback, B. G., Magoon, L. B., et al. (2013). Chemometric differentiation of crude oil families in the San Joaquin Basin. *California, American Association of Petroleum Geologists Bulletin*, 97(1), 103–143.
- Peters, K. E., Fraser, T. H., Amris, W., Rustanto, B., & Hermanto, E. (1999). Geochemistry of crude oils from Eastern Indonesia. *American Association of Petroleum Geologists Bulletin*, 83, 1927–1942.
- Peters, K. E., & Moldowan, J. M. (1991). Effects of source, thermal maturity, and biodegradation on the distribution and isomerization of homohopanes in petroleum. *Organic Geochemistry*, 17, 47–61.
- Peters, K. E., Ramos, L. S., Zumberge, J. E., Valin, Z. C., Scotese, C. R., & Gautier, D. L. (2007). Circum-Arctic petroleum systems identified using decision-tree chemometrics. *American Association of Petroleum Geologists Bulletin*, 91, 877–913.
- Peters, K. E., Walters, C. C., & Moldowan, J. M. (2005). *The biomarker guide* (2nd ed., p. 1155). Cambridge: Cambridge University Press.
- Peters, K. E., Wright, T. L., Ramos, L. S., Zumberge, J. E., & Magoon, L. B. (2016). Chemometric recognition of genetically distinct oil families in the Los Angeles basin, California. *American Association of Petroleum Geologists Bulletin*, 100, 115–135.
- Philp, R. P. (1985). *Fossil fuel biomarkers: Applications and spectra* (p. 294). Amsterdam: Elsevier Science Publishers B.V.
- Purser, B. H., & Bosence, D. W. J. (1998). Organization and scientific contributions in sedimentation and tectonics of rift basins: Red Sea-Gulf of Aden. In B. H. Purser & D. W. J. Bosence (Eds.), *Sedimentation and tectonics in rift basins* (pp. 3–8). London: Chapman and Hall.
- Radke, M., & Welte, D. H. (1983). The methylphenantrene index (MPI): a maturity parameter based on aromatic hydrocarbons. In M. Bjorøy, C. Albrecht, C. Cornford, K. de Groot, G. Eglinton, E. Galimov, D. Leythaeuser, R. Pelet, J. Rulkoetter, & G. Speers (Eds.), *Advances in organic geochemistry* (pp. 504–512). New York: Wiley.
- Richardson, M., & Arthur, M. A. (1988). The Gulf of Suez-northern Red Sea Neogene rift: A quantitative basin analysis. *Marine and Petroleum Geology*, 5(3), 247–270.
- Robinson, V., & Engel, M. (1993). Characterization of the source horizons within the Late Cretaceous transgressive sequence of Egypt. In B. Katz & L. Pratt (Eds.), *Source rocks in a sequence stratigraphic framework* (pp. 101–117). Tulsa: American Association of Petroleum Geologists, Studies in Geology.
- Robison, V. D. (1995). Source rock characterization of the Late Cretaceous Brown Limestone of Egypt. In B. Katz (Ed.), *Petroleum source rocks* (pp. 265–281). Berlin: Springer.
- Rohrbach, B.G. (1983). Crude oil geochemistry of the Gulf of Suez. In M. Bjorøy, C. Albrecht, C. Cornford, et al., (Eds.), *Advances in organic geochemistry, 1981* (pp. 39–48). Chichester: Wiley and Sons, Ltd.
- Rubinstein, I., Sieskind, O., & Albrecht, P. (1975). Rearranged sterenes in a shale: Occurrence and simulated formation. *Journal of the Chemical Society, Perkin Transactions*, 1, 1833–1836.
- Schütz, K. I. (1994). Structure and stratigraphy of the Gulf of Suez, Egypt. In S. M. Landon (Ed.), *Interior rift basins* (Vol. 59, pp. 57–96). Tulsa: American Association of Petroleum Geologists Memoir.
- Seifert, W. K., & Moldowan, J. M. (1978). Applications of steranes, terpanes and monoaromatics to the maturation, migration and source of crude oils. *Geochimica et Cosmochimica Acta*, 42, 77–95.
- Seifert, W. K., & Moldowan, J. M. (1979). The effect of biodegradation of steranes and terpanes in crude oils. *Geochimica et Cosmochimica Acta*, 43, 111–126.
- Seifert, W. K., & Moldowan, J. M. (1981). Paleoreconstruction by biological markers. *Geochimica et Cosmochimica Acta*, 45(6), 783–794.
- Seifert, W. K., & Moldowan, J. M. (1986). Use of biological markers in petroleum exploration. In R. B. Johns (Ed.), *Methods in geochemistry and geophysics* (Vol. 24, pp. 261–290). Amsterdam: Elsevier.
- Sellwood, B. W., & Netherwood, R. E. (1984). Facies evolution in the Gulf of Suez area: Sedimentation history as an indicator of rift initiation and development. *Modern Geology*, 9, 43–69.
- Sharaf, L. M., El Leboudy, M. M., & Shahin, A. N. (2007). Oil families and their potential sources in the southern Gulf of Suez. *Egypt. Petroleum Science and Technology*, 25, 539–559.
- Sinninghe Damsté, J. S., Eglinton, T. I., De Leeuw, J. W., & Schenck, P. A. (1989). Organic sulphur in macromolecular sedimentary organic matter: I. Structure and origin of sulphur-containing moieties in kerogen, asphaltenes and coal as revealed by flash pyrolysis. *Geochimica et Cosmochimica Acta*, 53(4), 873–889.

- Sinninghe Damsté, J. S., Kenig, F., Koopmans, M. P., Köster, J., Schouten, S., Hayes, J., et al. (1995). Evidence for gammacerane as an indicator of water column stratification. *Geochimica et Cosmochimica Acta*, 59, 1895–1900.
- Sofer, Z. (1980). Preparation of carbon dioxide for stable carbon isotope analysis of petroleum fractions. *Analytical Chemistry*, 52, 1389–1391.
- Sofer, Z. (1984). Stable carbon isotope composition of crude oils: Application to source depositional environments and petroleum alteration. *American Association of Petroleum Geologists Bulletin*, 68(1), 31–49.
- Steckler, M. S. (1985). Uplift and extension of the Gulf of Suez. *Nature*, 317, 135–139.
- Steckler, M. S., Berthelot, F., Lyberis, N., & Le Pichon, X. (1988). Subsidence in the Gulf of Suez: implications for rifting and plate kinematics. *Tectonophysics*, 153, 249–270.
- Subroto, E. A., Alexander, R., & Kagi, R. I. (1991). 30-Norhopanes: their occurrence in sediments and crude oils. *Chemical Geology*, 93, 179–192.
- ten Haven, H. L., de Leeuw, J. W., Rullkötter, J., & Sinninghe Damsté, J. S. (1987). Restricted utility of the pristane/phytane ratio as a palaeoenvironmental indicator. *Nature*, 330, 641–643.
- Thompson, K. F. M. (1983). Classification and thermal history of petroleum based on light hydrocarbons. *Geochimica et Cosmochimica Acta*, 47, 303–316.
- Thompson, K. F. M. (1987). Fractionated aromatic petroleum and the generation of gas–condensates. *Organic Geochemistry*, 11, 573–590.
- Tissot, B. P., & Welte, D. H. (1984). *Petroleum formation and occurrence* (p. 699). Berlin: Springer.
- Trendel, J.-M., Restlé, A., Connan, J., & Albrecht, P. (1982). Identification of a novel series of tetracyclic terpene hydrocarbons (C₂₄–C₂₇) in sediments and petroleum. *Journal of the Chemical Society, Chemical Communications*, 5, 304–306.
- Wang, Y.-P., Zhang, F., Zou, Y.-R., Zhan, Z.-W., & Peng, P. (2016). Chemometrics reveals oil sources in the Fangzheng Fault Depression, NE China. *Organic Geochemistry*, 102, 1–13.
- Wang, Y.-P., Zou, Y.-R., Shi, J.-T., & Shi, J. (2018). Review of the chemometrics application in oil-oil and oil-source rock correlations. *Journal of Natural Gas Geoscience*, 3, 217–232.
- Wever, H. E. (1999). A common source rock for Egyptian and Saudi hydrocarbons in the Red Sea: Discussion. *American Association of Petroleum Geologists Bulletin*, 83(5), 802–804.
- Wever, H. E. (2000). Petroleum and source rock characterization based on C₇ plot results: Examples from Egypt. *American Association of Petroleum Geologists Bulletin*, 84(7), 1041–1054.
- Younes, M. A. (2003). Hydrocarbon seepage generation and migration in the southern Gulf of Suez, Egypt: Insight from biomarker characteristics and source rock modeling. *Journal of Petroleum Geology*, 26(2), 211–224.
- Younes, A. I., & McClay, K. R. (2002). Development of accommodation zones in the Gulf of Suez—Red Sea rift, Egypt. *American Association of Petroleum Geologists Bulletin*, 86(6), 1003–1026.
- Younes, M. A., & Philp, R. P. (2005). Source rock characterization based on biological marker distributions of crude oils in the southern Gulf of Suez. *Egypt. Journal of Petroleum Geology*, 28(3), 301–317.
- Zein El Din, M. Y., Matbouly, S. I., Moussa, S. M., & Abdel Khalek, M. A. (1990). Geochemistry and oil-oil correlations in the Western Desert. In *Proceedings of the 10th Egyptian General Petroleum Corporation Exploration and Production Conference*, Cairo, Egypt, unpaginated.
- Zumberge, J. E. (1983). Tricyclic diterpane distributions in the correlation of Paleozoic crude oils from the Williston Basin. In M. Bjorøy (Ed.), *Advances in organic geochemistry* (pp. 738–745). New York: Wiley.
- Zumberge, J. E. (1987). Terpenoid biomarker distributions in low maturity crude oils. *Organic Geochemistry*, 11(6), 479–496.
- Zumberge, J. E., Russell, J. A., & Reid, S. A. (2005). Charging of Elk Hills reservoirs as determined by oil geochemistry. *American Association of Petroleum Geologists Bulletin*, 89, 1347–1371.